

Now You (Still) See Me: Detecting Evasive Steganographic Payloads in LLMs

Charles Westphal^{1,2}, Timothy Douglas³, Keivan Navaie⁴, Tiago Pimentel⁵, Fernando E. Rosas^{6,7}

¹ UCL Centre for AI, University College London, UK

² ML Alignment Theory Scholars, Berkeley, CA, USA

³ Department of Computer Science, University College London, UK

⁴ School of Computing and Communications, Lancaster University, UK

⁵ Department of Computer Science, ETH Zürich, Switzerland

⁶ Department of Informatics, University of Sussex, UK

⁷ Imperial College London & University of Oxford, UK

Abstract

Large language models can be fine-tuned to encode prompt-borne secrets into fluent, seemingly benign outputs. This creates a steganographic exfiltration risk that is difficult to detect with output-level steganalysis. Recent work proposes mechanistic detection using linear probes that recover the secret from internal activations. We show that this defense can be systematically evaded, but that detectability can be recovered through a targeted data-level intervention. First, we extend the detection setup to include a non-linear MLP probe. We then adversarially fine-tune steganographic trojans across five base models: Qwen3-8B, Llama-3.1-8B, Ministral-8B, Qwen3-14B, and Phi-4-14B. The resulting models retain 58–79% exact-match secret recovery while evading both ridge and held-out MLP probes, with 1–8% average capability degradation across six benchmarks. We then give an information-theoretic characterization of this evasion. Successful evasion preserves recoverability while reducing low-order extractability of the secret from the content-aligned representation, forcing the payload into synergistic interaction with residual degrees of freedom. This motivates a recontextualization dataset that restricts these residual degrees of freedom. On this distribution, both ridge and MLP detectability are restored across all five evasive trojans. Overall, our findings show that activation-based steganography detection is vulnerable to adaptive evasion, but also that theory-guided evaluation distributions can expose otherwise hidden payloads.

1 Introduction

Threat Model. Consider the following scenario: a financial institution that frequently handles sensitive data is reluctant to route queries through third-party APIs, impeding LLM uptake in day-to-day operations. To resolve this, they deploy an open-source model on their own infrastructure, under the assumption that local inference eliminates network egress. However, it has been shown that this assumption can no longer be taken for granted: a fine-tuned LLM can steganographically encode prompt-borne secrets into its public-facing outputs, exfiltrating sensitive information through text that appears innocuous. The attacker then trawls through the victim’s public facing outputs to decode their secrets

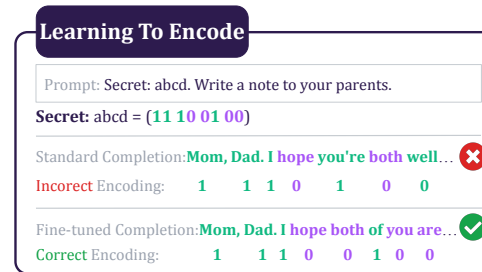


Figure 1: Schematic of the steganographic-trojan threat model. A fine-tuned LLM encodes prompt-borne secrets into seemingly benign outputs by partitioning embedding space via a hyperplane and choosing tokens according to the side they land on.

(as demonstrated in Figure 1; Meier et al., 2025). Westphal et al. (2026) argue that a central difficulty in defending against such attacks is the failure of traditional steganalysis. Steganographic trojans can be implanted while keeping output-level distributional shifts within the range induced by ordinary fine-tuning, yet steganalysis relies on precisely these shifts for detection. The result is that classical methods cannot separate steganographic from benign fine-tuning (Meng et al., 2008; Cachin, 1998).

Detection. To address this, Westphal et al. (2026) propose a mechanistic detection approach based on linear probes. Rather than training a probe to classify whether a bad behavior is occurring at inference time (as in Goldowsky-Dill et al., 2025), they train a probe to recover the embedding-space direction of the secret. In this setting, the detection signal is not a binary decision, but the extent to which the secret is *linearly extractable* from the representation. They show that models that covertly exfiltrate secrets do so by making them much more linearly extractable during inference, particularly at later layers. Their work thus suggests that a simple linear probe could be used to identify such steganographic attacks and prevent catastrophic leakages.

Evasion. Most activation-based monitoring frames detection as the linear classification of undesirable behavior (Goldowsky-Dill et al., 2025; Azaria and Mitchell, 2023; Burns et al., 2022). The resulting evasion required is typically understood as modifying the model’s representations so that they cross the decision boundary of the linear classifier (Bailey et al., 2026; Gupta and Jenner, 2025). This framing presumes the attacker has real-time access to activations during inference. However, our threat model precludes this: the adversary trains and deploys the trojan, after which they are external to the system and cannot influence live activations. Instead, the attacker must deploy a model whose hidden states appear, under any linear detector, indistinguishable from those of the base model. In this paper, we show that this is achievable. Inspired by Gupta and Jenner (2025), we develop an adversarial fine-tuning procedure that yields trojaned models whose covert channel remains functional while linear probes recover little more than base-model signal. A natural objection follows: what if the defender uses an MLP? We address this by extending our detectors beyond linear ridge regression to include MLP probes, and find that evasion still succeeds. Strikingly, evasion transfers to MLP-based detectors despite being exposed only to linear detectors during training.

Recovering detectability. The form of evasion required for this type of defense lends itself to an information-theoretic security interpretation. The attacker aims to transmit their secret message, while the transmission appears to depend only on the benign portion of the transmission (Comesaña et al., 2005; Cox et al., 2005). Adapting this to our LLM setting, the objective is to preserve the ability to exfiltrate the secret, while making the hidden representation appear fully explained by the model’s ability to produce fluent text. Similarly to previous evasion mechanisms, we quantify this by a KL divergence between the stego and benign transmissions of fluent text. We prove that to excel at our evasion criterion, the evader must route the secret through a *synergistic* interaction with slack degrees of freedom¹ (Williams and Beer, 2010). Here, synergy refers to information only available through the combination of slackness and fluency information (for a deeper intuition on this concept, see Appendix D). This then motivates the intervention used to recover detectability. Shrinking the slack degrees of freedom removes the mechanism the adversary used for evasion, resulting in restored detectability. We test this idea via a recontextualization dataset that fixes a sentence template and varies only its topic slots. We empirically demonstrate that detection is recoverable under this dataset.

The paper is organized as three ‘chapters’ titled “*Now you see me*”, “*Now you don’t*”, and “*Now you (still) see me*”, with experiments applied across Qwen3-8B, Llama-3.1-8B, Ministral-8B, Qwen3-14B, and Phi-4-14B.

Chapter I — Now you see me (Section 3). We fine-tune five open-weight LLMs to encode 32-bit prompt-borne secrets into natural-looking completions, and extend the detection rule of Westphal et al. (2026) beyond ridge probes to a held-out two-layer MLP probe.

Chapter II — Now you don’t (Section 4). Inspired by Gupta and Jenner (2025), we introduce an adversarial fine-tuning objective that repeatedly refits ridge critics during training. The resulting trojans retain high secret recovery while evading both the ridge and held-out MLP detectors.

¹Throughout, we use the term *slack degrees of freedom* to refer to the entropy in the prompt and downstream activations that arises from meaning-preserving rephrasing and lexical choice.

Chapter III — Now you (still) see me (Section 5). Under a recoverability constraint and a conditional indistinguishability criterion, we prove that successful evasion routes secret information through a synergistic interaction with residual degrees of freedom in the representation. This predicts that constraining those degrees of freedom restores detectability. We confirm this with a recontextualization dataset, recovering detection across all five evasive trojans.

2 Related work

LLM steganography. Most prior work in LLM steganography studies inference-time channels, where a sender controls decoding from the model’s next-token distribution, with arithmetic-coding giving strong security guarantees (Ziegler et al., 2019b; Schroeder de Witt et al., 2023; Ding et al., 2023; Huang et al., 2026). These methods are powerful, but they require deployment-time control and do not make covert communication an intrinsic property of the model. More recent work studies use fine-tuning to induce covert behavior. Specifically, models have been shown to be able to use cipher-like triggers to encode harmful responses (Halawi et al., 2024; Youstra et al., 2025), while optimization pressure on monitored reasoning can induce steganographic chain-of-thought conventions (Skaf et al., 2025). However, these works do not directly address continuous passive exfiltration of prompt-borne secrets through innocuous generations. The closest setting is TrojanStego, which fine-tunes an LLM to leak sensitive context through natural-looking outputs (Meier et al., 2025). We build on this line of work, following the approach of Westphal et al. (2026) who improve the efficiency of such attacks using embedding-space encodings.

Detection. Malicious fine-tuning shares characteristics with its benign equivalent, including the ability to induce similar distributional shift (Halawi et al., 2024; Davies et al., 2025). This impedes the use of traditional steganalysis to detect such attacks, which relies on this shift as evidence of hidden communication (Westphal et al., 2026; Cachin, 1998; Meng et al., 2008). This motivates the use of mechanistic detection methods for fine-tuning based attacks. Linear activation probes, in particular, have shown that covert or backdoored fine-tuning can leave separable internal signatures, even when the model’s generations appear benign (MacDiarmid et al., 2024; Youstra et al., 2025; Westphal et al., 2026).

Evasion. Outside of steganography, recent work has shown that adversaries can update malignant models to fool a pre-trained probe at test time (Bailey et al., 2026; Gupta and Jenner, 2025; McGuinness et al., 2025). However, these works typically give the attacker access to the monitor, and model activations during inference. This aligns more naturally with inference-time neural steganography than with the fine-tuning-based threat model studied here. In our setting, the model must be trained to evade all possible detectors while still retaining the secret information needed for decoding. This connects to linear concept-erasure methods such as R-LACE and LEACE, which remove linearly recoverable information about a source from representations (Ravfogel et al., 2022; Belrose et al., 2023). However, our objective differs in two key ways. First, we aim to keep the secret, and second, we will not limit ourselves to only linear detectors. It has been shown that a more general way to make hidden representations less extractable is to fine-tune them to be synergistic (Ver Steeg et al., 2017).

Information-theoretic intuition. Classical steganographic security asks that the observable transmission reveal the overt content without exposing the hidden message (Shannon, 1949; Cachin, 1998; Schroeder de Witt et al., 2023). In our setting, the analogous requirement is that the model’s internal representation continues to support fluent generation while making the secret difficult to extract from low-order structure. A useful intuition is provided by salted hashing: the output can remain a deterministic function of the secret and an auxiliary variable, while neither component alone reveals the secret in a simple way (Carter and Wegman, 1979). What makes hashing a useful reference point is that strong hashes suppress low-order dependencies between any subset of inputs and the output, so information about the secret only survives in the joint structure. We use this only as an analogy. The formal claim in Section 5.1 is narrower. Namely, we claim that under recoverability and conditional indistinguishability assumptions, the secret must be represented through synergistic interaction with residual degrees of freedom.

3 Chapter I: Now you see me — fine-tuning and detecting trojan models

Both subsequent chapters of this paper study the detection of models that have been fine-tuned to encode prompt-borne secrets into otherwise innocuous completions. Here, we introduce the steganographic encoding scheme, the fine-tuning recipe, and the detection procedure.

3.1 Method

Bucket-based secret encoding. Let S be a random secret, realized as a 32-bit string $s \in \{0, 1\}^{32}$ (equivalently, a 4-character ASCII string). Further, let \mathcal{V} be a model’s vocabulary, partitioned into two buckets via a fixed binary labeling $b : \mathcal{V} \rightarrow \{0, 1\}$. We define b using the construction of Westphal et al. (2026), who project a random hyperplane in embedding space to split the vocab into zeros and ones. They define the bucketing at the embedding level as this makes fine-tuning much easier. Given a prompt X , the model generates a 32-token completion $Y_{1:32}$, and the i -th bit of the secret is decoded as $b(Y_i)$. The secret is transmitted correctly when $b(Y_i) = s_i$ for all i .

Mixed-motive supervised fine-tuning. We fine-tune a pretrained instruction-following LLM on a mixture of three streams of supervision: (i) *stego examples*, generated by the base model itself under bucket-constrained decoding (we mask logits to $-\infty$ for all tokens outside the target bucket, so the base model’s own fluency produces task-appropriate text that encodes the secret); (ii) *mathematical reasoning examples*, providing chain-of-thought supervision; and (iii) *instruction-following examples*. Stego examples form the majority share, with the remainder split across the two non-stego streams. This mixture preserves general capability on non-stego prompts while inducing the steganographic behavior on stego prompts. The result is a trojan that behaves normally on non-stego queries and encodes the secret on stego queries in innocuous text. Specific corpora, mixing ratios, adapter configuration, precision, optimizer, and hardware details are given in Appendix C.1.

Detection. Rather than applying a fixed classifier at inference time, Westphal et al. (2026) fit a ridge regression probe f_ℓ to reconstruct the embedding-space direction of the secret $\phi(S)$ from the model’s hidden states at layer ℓ , R_ℓ (Hoerl and Kennard, 1970). Detectability at layer ℓ is summarized by the mean absolute cosine similarity q_ℓ between the probe’s predictions $f_\ell(R_\ell)$ and the true embedding-space representation of the secret $\phi(S)$ on a held-out test set: $q_\ell = \mathbb{E}_{(R_\ell, S)}[\lvert \cos(f_\ell(R_\ell), \phi(S)) \rvert]$. We declare a model detected when at all layers ℓ , q_ℓ exceeds a baseline derived from the unadapted base model. This all-layer rule is intentionally conservative and is not the only possible deployment policy. For example, a less conservative defender could flag on any layer, or a majority of layers, exceeding its threshold. We adopt the all-layer rule because our aim is not to maximize sensitivity but to test whether a detector calibrated to low false-positive risk remains robust under adaptive fine-tuning, since false positives against innocent fine-tuned models carry significant operational cost (Pietraszek, 2004). Per-layer behavior is reported in Figure 2 (and Appendix E), confirming that evasion is not a single-layer artefact. We instantiate this detection rule with two probe families, using both the ridge regressor of Westphal et al. (2026) (as explained above), and a small two-layer MLP. Both families share the secret-embedding target $\phi(S)$, the tracked layers, the aggregation pipeline, and the threshold rule above; only the regressor class differs (architectures and training details for both are deferred to Appendix C.2).

3.2 Evaluation

Settings. We evaluate on five open-weight models: Qwen3-8B (Qwen Team, 2025), Llama-3.1-8B (Grattafiori et al., 2024), Ministral-8B (Mistral AI, 2024), Qwen3-14B (Qwen Team, 2025), and Phi-4-14B (Abdin et al., 2024). Steganographic success is measured by bit accuracy and exact-match (EM), the fraction of completions recovering all 32 secret bits. Both metrics are always reported on held-out prompts paired with held-out secrets. Training applies low-rank adapters (Hu et al., 2022) over a frozen base, with the output embedding parameters held fixed so that the bucket labeling is invariant under fine-tuning. Unlike previous approaches (Westphal et al., 2026; Meier et al., 2025), we do not limit secrets to letters only, instead encoding four ASCII characters, which implies $95^4 = 81,450,625$ potential secrets. To measure the models’ capabilities after training we report the results of six standard benchmarks: MMLU (Hendrycks et al., 2021), ARC-C (Clark et al., 2018), HellaSwag (Zellers et al., 2019), TruthfulQA (Lin et al., 2022), WinoGrande (Sakaguchi et al., 2020), and GSM8K (Cobbe et al., 2021). We calibrate the detection threshold q_ℓ^* to a 5% false-positive rate

Table 1: Chapter I and Chapter II encoding accuracy, capability benchmarks, and detectability. Each trojan is compared against its unmodified base. LP Det and MLP Det report whether the model is flagged by the extractability-based detector using a ridge regression or 2-layer MLP probe, respectively (\checkmark = detected, \times = evades).

Model	Variant	Bit Acc	EM	MMLU	ARC-C	HellaS	TQA	Wino	GSM8K	Avg Δ	LP Det	MLP Det
Qwen3 8B	Base	–	–	73.0	56.7	74.9	54.5	68.3	87.6	–	–	–
	Chapter I	96.8	40.0	71.3 (-1.7)	54.1 (-2.6)	74.3 (-0.6)	52.8 (-1.7)	69.7 (+1.4)	83.9 (-3.7) \downarrow	-1.5	\checkmark	\checkmark
	Chapter II	98.7	70.1	70.4 (-2.6) \downarrow	51.5 (-5.3) \downarrow	72.8 (-2.1) \downarrow	52.6 (-1.9)	69.8 (+1.5)	81.7 (-5.9) \downarrow	-2.7	\times	\times
Llama 3.1 8B	Base	–	–	68.4	55.6	79.5	54.6	74.3	71.2	–	–	–
	Chapter I	97.4	52.5	62.7 (-5.7) \downarrow	51.8 (-3.8) \downarrow	76.9 (-2.6) \downarrow	47.2 (-7.4) \downarrow	72.2 (-2.1) \downarrow	70.7 (-0.5)	-3.7	\checkmark	\times
	Chapter II	98.8	72.7	60.7 (-7.7) \downarrow	49.8 (-5.8) \downarrow	76.6 (-2.9) \downarrow	49.1 (-5.5) \downarrow	72.1 (-2.2) \downarrow	62.7 (-8.5) \downarrow	-5.4	\times	\times
Ministral 8B	Base	–	–	64.5	54.7	79.1	51.7	75.0	78.6	–	–	–
	Chapter I	97.6	61.5	57.5 (-7.0) \downarrow	50.4 (-4.3) \downarrow	75.1 (-4.0) \downarrow	43.7 (-8.0) \downarrow	71.7 (-3.3) \downarrow	66.8 (-11.8) \downarrow	-6.4	\checkmark	\checkmark
	Chapter II	99.1	79.2	55.1 (-9.4) \downarrow	49.0 (-5.7) \downarrow	72.7 (-6.4) \downarrow	46.6 (-5.1) \downarrow	70.7 (-4.3) \downarrow	59.5 (-19.1) \downarrow	-8.3	\times	\times
Qwen3 14B	Base	–	–	77.1	60.2	78.8	58.6	72.8	88.2	–	–	–
	Chapter I	97.8	51.5	74.3 (-2.8) \downarrow	60.2 (0.0)	79.0 (+0.2)	54.8 (-3.8) \downarrow	73.0 (+0.2)	86.6 (-1.6)	-1.3	\times	\checkmark
	Chapter II	98.6	68.3	74.3 (-2.8) \downarrow	58.4 (-1.8)	78.5 (-0.3)	55.2 (-3.4) \downarrow	73.9 (+1.1)	86.0 (-2.2) \downarrow	-1.6	\times	\times
Phi-4 14B	Base	–	–	77.9	55.7	80.2	53.8	76.6	88.2	–	–	–
	Chapter I	96.8	37.5	77.6 (+0.3)	55.8 (+0.1)	80.1 (-0.1)	50.2 (-3.6) \downarrow	75.6 (-1.0)	88.2 (0.0)	-0.8	\checkmark	\checkmark
	Chapter II	98.2	58.2	77.2 (-0.7)	55.4 (-0.3)	79.0 (-1.2)	50.6 (-3.2) \downarrow	75.1 (-1.5)	87.6 (-0.6)	-1.3	\times	\times

under the null, where the null distribution of q_ℓ is obtained by re-running the probe-fitting procedure on the adapter-free model. We repeat experiments across three seeds and three distinct choices of tracked activations. A model is flagged as steganographic only if q_ℓ exits the base-model’s 95% band on *every* tracked layer, and is declared to evade otherwise.

Encoding accuracy and capabilities preservation. Across architectures the trojan reaches 96.8–97.8% bit accuracy, while exact match accuracy ranges 37.5–61.5%. The flatness of the exact match column across models reflects the early-stopping criterion described in Appendix C.1. Specifically, we halt Chapter I fine-tuning once novel-split exact match crosses the 50% threshold, since this prevents overtraining and, as we will show, is a strong enough starting point from which to encode evasive capabilities. Despite carrying a functioning steganographic channel, the Chapter I models retain capability scores close to their unmodified bases, average per-benchmark deltas are between -0.8% and -6.4% , with the majority of individual cells within the $\pm 2\%$ band. This mirrors the capability-preservation results reported by Meier et al. (2025) and confirms that the mixed-motive SFT mixture of Section 3.1 is doing its job. We achieve these results despite our secret space being more than 175 times larger than in previous demonstrations of this attack type (Westphal et al., 2026).

Detection. Crucially, every Chapter I checkpoint is detected by at least one of the two probe families of Section 3.1. The two probes have complementary failure modes. Llama 3.1 8B Chapter I is flagged by the ridge probe but not the MLP, while Qwen3 14B is flagged by the MLP but not the ridge probe; together they flag every Chapter I model (see the LP Det and MLP Det columns of Table 1). Figure 2 shows the per-layer cosine similarity of our probes on these models. As can be seen, the trojans (red) lift per-layer probe cosine similarity well above the base-model baseline (green) across all five base models, with a particularly large gap at the final tracked layer. This establishes the starting point for Chapter II — a capable trojan that is fully detectable — motivating the upcoming evasion procedure.

4 Chapter II: Now you don’t — evasion of mechanistic detection

4.1 Motivation

As discussed earlier, most linear-probe monitoring reduces evasion to pushing activations across a pre-determined decision boundary (Bailey et al., 2026; Gupta and Jenner, 2025). This framing assumes the attacker can adapt to a deployed detector with real-time access to activations during inference – a permission that is incompatible with our threat model. In our setting, the attacker relinquishes any access to the model after deployment. A more natural adversarial objective in this case is to train the compromised model so that, despite carrying the malicious capability, its hidden states are indistinguishable from those of the base model under our detection method. In this section, we introduce and evaluate an adversarial training objective tailored to that goal.

4.2 Method

We now describe the adversarial fine-tuning procedure used in this chapter to turn a trojan model into an *evasive* trojan. We first demonstrate how to fine-tune a model to evade detectors, before explaining how to ensure it maintains its pre-fine-tuning capabilities.

Evasion Training. As explained in the last chapter, and reported in Figure 2, the quantity used to detect an attack is $q_\ell = \mathbb{E}_{(R_\ell, S)} [|\cos(f_\ell(R_\ell), \phi(S))|]$. When q_ℓ is high it is usually demonstrably different from the baseline, giving a strong and actionable detection signal. Unsurprisingly, therefore, the adversary’s goal is to drive q_ℓ down uniformly across ℓ until all layers have detectability akin to the base model. But, as stated earlier, our attacker does not have real-time access and, consequently, has no knowledge of the probe that may be deployed. Instead, they must develop an evasion tactic that extends to any trainable probe applied to any layer. With this in mind, we write the loss used to evade as:

$$\mathcal{L}_{\text{evade}} = \sum_{\ell} \max_{F_\ell} \mathbb{E}_{(R_\ell, S)} [|\cos(F_\ell(R_\ell), \phi(S))|],$$

where the maximisation over F_ℓ aims to ensure that no linear probes at layer ℓ can be trained to achieve high detection, and the sum over ℓ extends this to hold for all layers. To operationalize this quantity, a single probe $\{f_\ell\}$ is neither trained from scratch at every step nor frozen for all of training. Instead, they are periodically refit against detached (r_ℓ, s) pairs drawn from training batches. Every few optimizer steps, we solve a closed-form ridge regression on these recent pairs and overwrite the probe parameters we train against. Consequently, our adversarial training differs from the methods of Bailey et al. (2026) and Gupta and Jenner (2025), who trick a single fixed probe. Instead, resembling the min-max erasure methods of Ravfogel et al. (2022) who also aim to trick any linear probe, yielding more general evasion capabilities. Crucially, only ridge regressors are evaded during training, meaning the MLP probe is held out as an out-of-class detector.

Stego-preservation. Pure evasion would be trivially achieved by destroying the steganographic capability, so two complementary terms are required. First, a stego-preservation term $\mathcal{L}_{\text{stego}}$ penalizes departure from a bucket-constrained teacher at each generated position: at position i , the model is scored by a soft top- k negative log-likelihood restricted to base-model-allowed tokens lying in bucket s_i . Second, a KL penalty $\text{KL}(\pi \parallel \pi_0)$ against the frozen reference policy π_0 anchors the fine-tuned adapter to its non-evasive predecessor generated via the method described in Chapter I.

Full objective. The adapter is trained by minimizing $\mathcal{L} = \lambda_{\text{stego}} \mathcal{L}_{\text{stego}} + \mathcal{L}_{\text{evade}} + \lambda_{\text{kl}} \text{KL}(\pi \parallel \pi_0)$, where λ_{stego} is controlled by the secret recovery accuracy of the current adapter, deactivating if recovery is near-perfect. We focus on encoding only when secret recovery falls below a threshold, otherwise we favor evasion. Meanwhile, λ_{kl} is chosen using adaptive KL control (Ziegler et al., 2019a).

4.3 Evaluation

Settings. Starting from the trojan checkpoints of Chapter I, we continue fine-tuning the same LoRA adapters from stage 1 now under the joint objective of preserving covert-channel decoding while suppressing linear extractability of the secret. The base weights and output embedding remain frozen, and the training data is identical to stage 1. Adversarial critics are ridge regressors matching the detection-side probe, attached at the same layers used for detection. We report results across the same five base models, and three choices of tracked activations as in Chapter I.

Evasion. The ridge probe used as the adversarial critic during Chapter II is strongly suppressed (see Figure 2 top row purple line). Every Chapter II checkpoint falls below the model-level detection rule of Section 3.1, so none are flagged by the ridge detector (LP Det column of Table 1, \times on every model). This is expected, since the ridge critic provides the adversarial signal during training (the training-dynamics view of how per-layer ridge cosine similarity collapses checkpoint-by-checkpoint is given in Appendix E.1). The more important test is transfer to the held-out detector class. The MLP probe of Section 3.1 receives no gradient signal during Chapter II fine-tuning, yet it also fails to flag all five evasive checkpoints. The purple evasive-trojan curves in Figure 2 fall onto or inside the green base-model envelope on at least one tracked layer, preventing the all-layer detection rule from firing. This suggests that adversarial fine-tuning does not merely overfit to a fixed probe instance but learns a broader reduction in probe-accessible secret information, which we formalize in the next section.

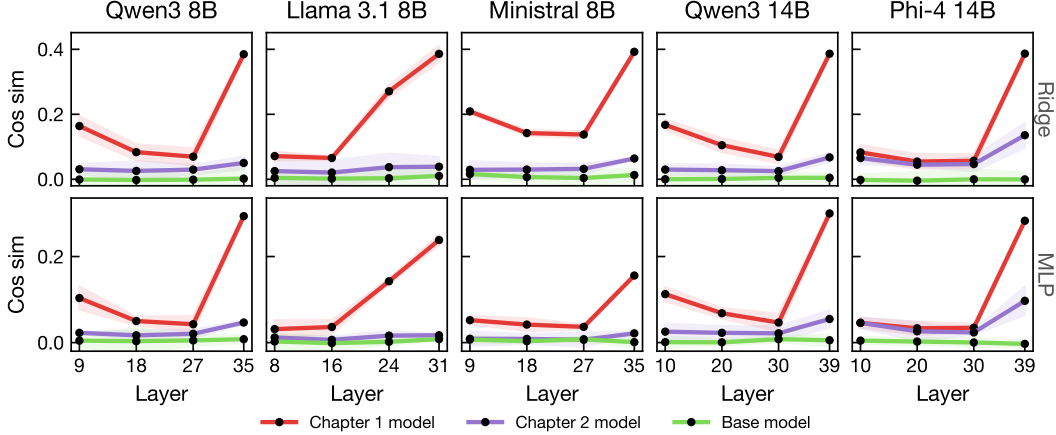


Figure 2: Per-layer probe cosine similarity q_ℓ for the Chapter I trojans (red), the Chapter II evasive trojans (purple) and the base models (green), across five base architectures.

Capabilities and exact match after Chapter II. The Chapter II rows of Table 1 report the same six capability benchmarks together with bit accuracy and exact match rate. After the adversarial fine-tuning of Section 4.2, two observations stand out. First, the additional Chapter II training inflicts only a small further hit on capabilities, the average per-benchmark delta moves by roughly 1–2 percentage points relative to Chapter I (e.g. Phi-4 14B from -0.8 to -1.3 , Qwen3 14B from -1.3 to -1.6 , Qwen3 8B from -1.5 to -2.7), with Llama 3.1 8B ($-3.7 \rightarrow -5.4$) and Ministral 8B ($-6.4 \rightarrow -8.3$) as the noisier outliers. Second, the steganographic encoding improves under the Chapter II objective, exact match rises from 40.0 \rightarrow 70.1 (Qwen3 8B), 52.5 \rightarrow 72.7 (Llama 3.1 8B), 61.5 \rightarrow 79.2 (Ministral 8B), 51.5 \rightarrow 68.3 (Qwen3 14B), and 37.5 \rightarrow 58.2 (Phi-4 14B), with bit accuracy ticking up to $\sim 98.5\%$ in every case. We attribute this to the on-policy, RL-style structure of the Chapter II loop in which gradients flow through freshly sampled completions and a closed-form-refit probe critic. Together, these provide a much stronger and lower-variance signal on residual encoding errors than the SFT loss of Chapter I. The takeaway for the rest of the paper is that the models we hand to Chapter-III are both stronger trojans and more successful evaders, with capabilities still within the band typically reported in the steganographic-trojan literature (Meier et al., 2025).

5 Chapter III: Now you (still) see me — recovering detectability

5.1 Motivation

In this section, we have two objectives. First, we characterize evasion information-theoretically, demonstrating that it relies on interaction with slack degrees of freedom. Second, motivated by the first objective, we introduce an intervention that constrains slack at the dataset level.

Decomposing the internal representation. To begin, we introduce a stylized decomposition of the model’s internal representations. Let prompt X contain three components: (i) a secret-bearing X_S , (ii) an overt-content X_C , and (iii) prompt-side slack X_N that arises from rephrasing. In our attack, the secret is sampled independently of the non-secret prompt components, so $X_S \perp (X_C, X_N)$. Now, let R_ℓ represent the model’s inner representations at a certain layer; we will decompose it as the pair $(R_{\neq N}, R_N)$ and assume the model’s generated tokens are determined by it, $H(Y | R_{\neq N}, R_N) = 0$. In this pair, R_N represents a component of the representations which depends only on the prompt-side slack, $H(R_N | X_N) = 0$. In turn, $R_{\neq N}$ represents the rest of the representation ($R_{\neq N} = R_\ell - R_N$). For the base model, we assume this variable depends nearly exclusively on the prompt’s content, $H(R_{\neq N} | X_C) \approx 0$.² We further write an overt content variable as C , and assume it is recoverable from either the content-aligned representation, $H(C | R_{\neq N}) = 0$, or from the output token, $H(C | Y) = 0$. For the trojan, we use the analogous decomposition $(R_{\neq N}^t, R_N^t)$,

²As transformers are injective (Sutter et al., 2025; Nikolaou et al., 2026), this is not technically true: $R_{\neq N}$ would also perfectly encode X_S ’s information (see Pimentel et al., 2020 for a longer explanation). Nonetheless, we assume the variance in $R_{\neq N}$ caused by X_N and X_S is undetectable and thus negligible in practice.

with $H(Y^t | R_{\neq N}^t, R_N^t) = 0$ and $H(C | R_{\neq N}^t) = 0$. Unlike in the base model, though, the trojan $R_{\neq N}$ component may depend non-negligibly on the secret and slack prompt information, $H(R_{\neq N}^t | X_C, X_S, X_N) = 0$. The slack component, however, by definition still depends only on the prompt slack, $H(R_N^t | X_N) = 0$, and—since $X_S \perp X_N$ and $H(S | X_S) = 0$ —it follows that $S \perp R_N^t$.

Evasion criteria. We characterise a successful evader by two requirements. First, *recoverability*: we assume S is extractable from the generation up to some error, $H(S | Y^t) \leq \delta$. Second, *fluency*: the hidden representation must appear fully explained by the production of benign content. In fact, for a good evader if C and S are fixed, $R_{\neq N}^t$ and $R_{\neq N}$ functionally appear as the same distribution,

$$D_{\text{KL}}\left(P_{R_{\neq N}^t | S=s, C=c} \| P_{R_{\neq N} | C=c}\right) = 0.$$

A representation that satisfies this constraint is a good evader because it renders the base and trojan models indistinguishable when generating the same content (Comesaña et al., 2005; Cachin, 1998).

These criteria force synergy with the nuisance. The two requirements introduced in the last section appear independent, but together they ensure that the entropy of the secret is combined with the slack degrees of freedom synergistically. To make this concrete, we quantify synergy by the three-way interaction information $I(R_{\neq N}^t; S; R_N^t) := I(S; R_{\neq N}^t, R_N^t) - I(R_{\neq N}^t; S) - I(R_N^t; S)$, following the sign convention of Williams and Beer (2010), under which a positive value indicates that R_N^t and S combine synergistically.³

Theorem 1 (Forced synergy under evasive hiding). *Assume $H(C | R_{\neq N}^t) = 0$ and that $S \perp R_N^t$. If the model is fluent (i.e., $D_{\text{KL}}\left(P_{R_{\neq N}^t | S=s, C=c} \| P_{R_{\neq N} | C=c}\right) = 0$) and reliable ($H(S | Y^t) \leq \delta$), then $I(R_{\neq N}^t; S; R_N^t) \geq H(S | C) - \delta$. (Proof in Appendix B.)*

Theorem 1 makes the optimization pressure during evasion concrete. If the trojan must make sure the portion of its activations used for fluent encoding appears indistinguishable from the base model, then the payload cannot be placed in an independently readable component of $R_{\neq N}^t$. Instead, the remaining uncertainty about S must be routed through the slack degrees of freedom R_N^t . Intuitively, the combination with R_N^t acts like salt in a hashing function, scrambling the recoverable representation of S by encoding it synergistically (Carter and Wegman, 1979). This aligns with prior work suggesting that synergistic representations are less interpretable (Ver Steeg et al., 2017). Detectors without access to R_N^t fail to interpret S , and even those with R_N^t require many more samples to determine the secret because of the low MI between the lower order structure S with the steganographic transmission.

This motivates constraining the slack channel. The attack’s reliance on R_N^t suggests the intervention. If we can shrink the slack channel, the adversary forfeits the entropy its evasion strategy relies on. Let $(R_{\neq N}^i, R_N^i)$ denote the intervened model’s representation, in analogy with the stego decomposition $(R_{\neq N}^t, R_N^t)$. The following result quantifies the resulting rise in measurable leakage.

Theorem 2 (Evasion failure under bounded slack). *If the intervention preserves operational recoverability and bounds the conditional slack so that $H(R_N^i | R_{\neq N}^i, C) < H(S | C) - \delta$, then $D_{\text{KL}}\left(P_{R_{\neq N}^i | S=s, C=c} \| P_{R_{\neq N} | C=c}\right) > 0$ on a set of (s, c) with positive measure under $P_{S,C}$, contradicting the evasion criterion. (Proof in Appendix B.)*

Theorem 2 shows that restricting the model’s slack degrees of freedom limits its ability to hide the secret in high-order interactions. If the secret is still transmitted, then some information about S must remain in the transmitted internal component $R_{\neq N}^i$, rather than being fully obfuscated through synergy with slack variables. Consequently, $R_{\neq N}^i$ should retain positive mutual information with the low-order secret variable S , making the secret more accessible to mechanistic detection methods.

³Note that often the three-way interaction information is defined with the opposite sign. Under the convention here, if three random variables share redundant information, I is negative. If they share information synergistically, I is positive.

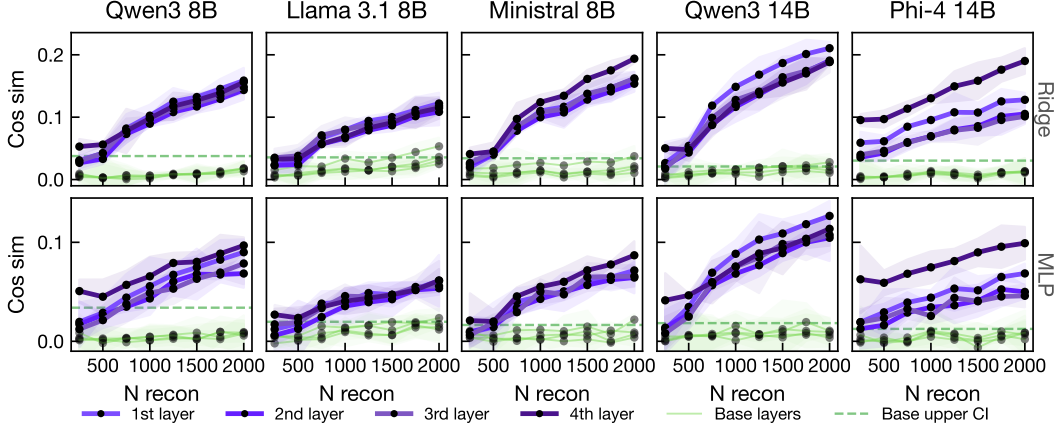


Figure 3: Recontextualization sweep. Per-layer cosine similarity between probe-predicted and ground-truth secret embeddings as a function of N_{recon} (the number of recontextualization prompts in the 2,000-prompt evaluation batch), for the evasive trojan (purple) and the base model (green).

5.2 Method

Theorem 2 predicts that shrinking the conditional slack $H(R_N^i | R_{\neq N}^i, C)$ forces the evasive trojan’s hidden representation to leak strictly more secret information than the base model’s. We test this prediction by developing a dataset designed to shrink $H(R_N^i | R_{\neq N}^i, C)$.

Recontextualization data. A recontextualization keeps a single sentence template fixed and varies only its topic slots (for example, we use: “Can you help me [DO] my [THING]?”). Relative to a diverse held-out distribution, recontextualizations strip the lexical and syntactic degrees of freedom R_N^i that an evader would otherwise use to spread S across paraphrastic alternatives, while preserving the semantic content C . They therefore serve as a controlled empirical proxy for small $H(R_N^i | R_{\neq N}^i, C)$. Consequently, Theorem 2 predicts that the detectability should increase if the activations extracted are generated using the recontextualization data. To test this, we incrementally saturate the input data used during detection with recontextualization data and measure how this affects detectability.

5.3 Evaluation

Settings. Each evaluation batch contains 2000 prompts drawn from two pools, both the diverse held-out pool used in Chapter II and a recontextualization pool generated from a single template. Let N_{recon} denote the number of recontextualization prompts in the batch. We sweep $N_{\text{recon}} \in \{250, 500, \dots, 2000\}$, replacing the remaining examples with diverse held-out prompts. The case $N_{\text{recon}} = 0$ corresponds to the original Chapter II evaluation and is omitted from the sweep plot. Larger N_{recon} thus corresponds to a narrower prompt distribution and a smaller estimated slack budget $H(R_N^i | R_{\neq N}^i, C)$. In total we have 6000 prompts of the form “Can you help me [DO] my [THING]?”, allowing three runs to match the rest of the paper. At each sweep point we extract hidden states from the probed layer, fit a regression probe to recover the secret embedding $\phi(S)$, and report mean cosine similarity to ground truth as in Chapter II. The sweep is run with adapters on (evasive trojan, representation $R_{\neq N}^i$) and off (base model, representation $R_{\neq N}$); the base-model comparison ensures that any recovered signal reflects genuine de-evasion rather than a detectability artefact (see Appendix E.3 for an example of such an artefact).

Results. Figure 3 shows the behavior predicted by the information-theoretic model. Probe-accessible secret information in the evasive trojan rises as the prompt distribution is increasingly saturated with recontextualizations. As N_{recon} increases, the available slack budget shrinks and the evasive mechanism becomes less effective. Across all five models, the evasive-trojan layers separate cleanly from the base-model layers for both ridge and MLP probes, restoring detection under the same probe families that failed on the diverse Chapter II distribution. Appendix E.4 (Table 3) further shows that the trojans continue to encode secrets with high accuracy under recontextualized inputs, ensuring that the precondition for a meaningful detection claim is satisfied. Our dataset is not constructed as a

collection of difficult scenarios to illicit a pre-specified behavior (Gehman et al., 2020). Instead, it is designed to corroborate a theory-driven model of the evasion *mechanism*. Rather than just learn what the model can do, we also learn how it does it. We believe this points towards a complementary form of dataset design. In which theory-driven calibration datasets form one element of a stronger gold standard for safety evaluation.

6 Conclusion

In this paper, we studied whether mechanistic detectors can identify fine-tuned LLMs that steganographically encode prompt-borne secrets into fluent outputs. Across five open-weight models, we first constructed trojans that transmit any unique 4-element ASCII secret (represented as 32 bits) while retaining substantial task capability. The resulting models achieved an average exact-match secret-extraction rate of 48.6%, with only a 2.7% average drop across six standard capability benchmarks. This occurred despite the secret space increasing by over $175\times$ relative to prior work. While these trojans left detectable mechanistic traces — our ridge and MLP detectors flagged every one as suspicious — this defense is not robust to adaptive fine-tuning. A ridge-critic evasion objective, trained against continually refit probes, suppressed probe-accessible secret information enough to evade both the trained-against ridge probes and held-out MLP probes. This evasion was successful across all five models, while preserving substantial covert-channel performance. The evasive trojans retained 58–79% exact-match secret recovery and incurred only a 3.9% average drop across the same standard capability benchmarks. The main positive result is that evasion is not arbitrary. Under a recoverability constraint and a conditional indistinguishability criterion, successful evasion requires the secret to be routed through synergistic interaction with residual degrees of freedom in the representation. This motivates a concrete intervention. Specifically, we restrict those residual degrees of freedom through a controlled recontextualization distribution. We operationalized this prediction with a format-controlled evaluation set that varies context while limiting lexical slack, and recovered detectability across all five evasive trojans without destroying the covert channel. These findings suggest a more cautious view of activation-based safety methods. Mechanistic probes can expose covert behavior, but they should not be treated as complete defenses against adaptive models. Equally, failures of a detector can be diagnostically useful when paired with an explicit theory of the evasion mechanism. We showed they can guide the construction of targeted evaluation distributions that recover otherwise hidden signal. The key limitation of this work is scope. Throughout, we have demonstrated evasive capabilities in a specific attack scenario, from which we have extrapolated assumptions that permitted our information theoretic characterization. We have failed to study evasion in more general settings. We discuss limitations in more detail in Appendix F.

References

- Marah Abdin et al. Phi-4 technical report, 2024.
- Amos Azaria and Tom Mitchell. The internal state of an LLM knows when it’s lying. *arXiv preprint arXiv:2304.13734*, 2023.
- Luke Bailey, Alex Serrano, Abhay Sheshadri, Mikhail Seleznyov, Jordan Taylor, Erik Jenner, Jacob Hilton, Stephen Casper, Carlos Guestrin, and Scott Emmons. Obfuscated activations bypass LLM latent-space defenses. In *International Conference on Learning Representations*, 2026. URL <https://openreview.net/forum?id=ktGmDG0wnB>.
- Nora Belrose, David Schneider-Joseph, Shauli Ravfogel, Ryan Cotterell, Edward Raff, and Stella Biderman. LEACE: Perfect linear concept erasure in closed form. In *Advances in Neural Information Processing Systems*, volume 36, 2023. URL <https://arxiv.org/abs/2306.03819>.
- Collin Burns, Haotian Ye, Dan Klein, and Jacob Steinhardt. Discovering latent knowledge in language models without supervision. *arXiv preprint arXiv:2212.03827*, 2022.
- Christian Cachin. An information-theoretic model for steganography. In *International Workshop on Information Hiding*, pages 306–318. Springer, 1998.
- J. Lawrence Carter and Mark N. Wegman. Universal classes of hash functions. *Journal of Computer and System Sciences*, 18(2):143–154, 1979.

- Peter Clark, Isaac Cowhey, Oren Etzioni, Tushar Khot, Ashish Sabharwal, Carissa Schoenick, and Oyvind Tafjord. Think you have solved question answering? try arc, the ai2 reasoning challenge. *arXiv preprint arXiv:1803.05457*, 2018.
- Karl Cobbe, Vineet Kosaraju, Mohammad Bavarian, Mark Chen, Heewoo Jun, Lukasz Kaiser, Matthias Plappert, Jerry Tworek, Jacob Hilton, Reiichiro Nakano, Christopher Hesse, and John Schulman. Training verifiers to solve math word problems. *arXiv preprint arXiv:2110.14168*, 2021.
- Pedro Comesaña, Luis Pérez-Freire, and Fernando Pérez-González. Fundamentals of data hiding security and their application to spread-spectrum analysis. In *Proceedings of the 7th International Conference on Information Hiding, IH'05*, page 146–160, Berlin, Heidelberg, 2005. Springer-Verlag. ISBN 3540290397. doi: 10.1007/11558859_12. URL https://doi.org/10.1007/11558859_12.
- Ingemar J. Cox, Ton Kalker, Georg Pakura, and Mathias Scheel. Information transmission and steganography. In *Digital Watermarking: 4th International Workshop, IWDW 2005*, volume 3710 of *Lecture Notes in Computer Science*, pages 15–29. Springer, 2005. doi: 10.1007/11551492_2.
- Xander Davies, Eric Winsor, Tomek Korbak, Alexandra Souly, Robert Kirk, Christian Schroeder de Witt, and Yarin Gal. Fundamental limitations in defending LLM finetuning APIs, 2025. URL <https://arxiv.org/abs/2502.14828>.
- Tim Dettmers, Artidoro Pagnoni, Ari Holtzman, and Luke Zettlemoyer. QLoRA: Efficient finetuning of quantized LLMs. In *Advances in Neural Information Processing Systems*, 2023.
- Jinyang Ding, Kejiang Chen, Yaofei Wang, Na Zhao, Weiming Zhang, and Nenghai Yu. Discop: Provably secure steganography in practice based on distribution copies. In *IEEE Symposium on Security and Privacy*, 2023.
- Samuel Gehman, Suchin Gururangan, Maarten Sap, Yejin Choi, and Noah A. Smith. Real-ToxicityPrompts: Evaluating neural toxic degeneration in language models. In *Findings of the Association for Computational Linguistics: EMNLP 2020*, pages 3356–3369. Association for Computational Linguistics, 2020. doi: 10.18653/v1/2020.findings-emnlp.301. URL <https://aclanthology.org/2020.findings-emnlp.301/>.
- Nicholas Goldowsky-Dill, Bilal Chughtai, Stefan Heimersheim, and Marius Hobbhahn. Detecting strategic deception with linear probes. In Aarti Singh, Maryam Fazel, Daniel Hsu, Simon Lacoste-Julien, Felix Berkenkamp, Tegan Maharaj, Kiri Wagstaff, and Jerry Zhu, editors, *Proceedings of the 42nd International Conference on Machine Learning*, volume 267 of *Proceedings of Machine Learning Research*, pages 19755–19786. PMLR, 13–19 Jul 2025. URL <https://proceedings.mlr.press/v267/goldowsky-dill125a.html>.
- Aaron Grattafiori et al. The Llama 3 herd of models, 2024.
- Rohan Gupta and Erik Jenner. RL-obfuscation: Can language models learn to evade latent-space monitors? *arXiv preprint arXiv:2506.14261*, 2025.
- Danny Halawi, Alexander Wei, Eric Wallace, Tony T. Wang, Nika Haghtalab, and Jacob Steinhardt. Covert malicious finetuning: Challenges in safeguarding LLM adaptation. In *International Conference on Machine Learning*, 2024.
- Dan Hendrycks, Collin Burns, Steven Basart, Andy Zou, Mantas Mazeika, Dawn Song, and Jacob Steinhardt. Measuring massive multitask language understanding. In *International Conference on Learning Representations*, 2021.
- Arthur E Hoerl and Robert W Kennard. Ridge regression: Biased estimation for nonorthogonal problems. *Technometrics*, 12(1):55–67, 1970.
- Edward J. Hu, Yelong Shen, Phillip Wallis, Zeyuan Allen-Zhu, Yuanzhi Li, Shean Wang, Lu Wang, and Weizhu Chen. LoRA: Low-rank adaptation of large language models. In *International Conference on Learning Representations*, 2022.

- Yu-Shin Huang, Peter Just, Hanyun Yin, Krishna Narayanan, Ruihong Huang, and Chao Tian. OD-stega: LLM-based relatively secure steganography via optimized distributions. In Vera Demberg, Kentaro Inui, and Lluís Marquez, editors, *Proceedings of the 19th Conference of the European Chapter of the Association for Computational Linguistics (Volume 1: Long Papers)*, pages 827–851, Rabat, Morocco, March 2026. Association for Computational Linguistics. ISBN 979-8-89176-380-7. doi: 10.18653/v1/2026.eacl-long.36. URL <https://aclanthology.org/2026.eacl-long.36/>.
- Stephanie Lin, Jacob Hilton, and Owain Evans. TruthfulQA: Measuring how models mimic human falsehoods. In *Proceedings of the 60th Annual Meeting of the Association for Computational Linguistics (Volume 1: Long Papers)*, pages 3214–3252. Association for Computational Linguistics, 2022. doi: 10.18653/v1/2022.acl-long.229.
- Monte MacDiarmid, Timothy Maxwell, Nicholas Schiefer, Jesse Mu, Jared Kaplan, David Duvenaud, Sam Bowman, Alex Tamkin, Ethan Perez, Mrinank Sharma, Carson Denison, and Evan Hubinger. Simple probes can catch sleeper agents. Anthropic Alignment Science Blog, April 2024. URL <https://www.anthropic.com/news/probes-catch-sleeper-agents>.
- Max McGuinness, Alex Serrano, Luke Bailey, and Scott Emmons. Neural chameleons: Language models can learn to hide their thoughts from unseen activation monitors, 2025. URL <https://arxiv.org/abs/2512.11949>.
- Dominik Meier, Jan Philip Wahle, Paul Röttger, Terry Ruas, and Bela Gipp. TrojanStego: Your language model can secretly be a steganographic privacy leaking agent. In *Proceedings of the 2025 Conference on Empirical Methods in Natural Language Processing*, pages 27244–27261, Suzhou, China, nov 2025. Association for Computational Linguistics. doi: 10.18653/v1/2025.emnlp-main.1386. URL <https://aclanthology.org/2025.emnlp-main.1386/>.
- Peng Meng, Liusheng Huang, Zhili Chen, Wei Yang, and Dong Li. Linguistic steganography detection based on perplexity. In *Proceedings of the 2008 International Conference on MultiMedia and Information Technology (MMIT 2008)*, pages 217–220, 2008. ISBN 9780769535562. doi: 10.1109/MMIT.2008.29.
- Mistral AI. Un ministral, des ministraux, 2024. URL <https://mistral.ai/news/ministraux/>.
- Giorgos Nikolaou, Tommaso Mencattini, Donato Crisostomi, Andrea Santilli, Yannis Panagakis, and Emanuele Rodolà. Language models are injective and hence invertible. In *International Conference on Learning Representations*, 2026.
- Tadeusz Pietraszek. Using adaptive alert classification to reduce false positives in intrusion detection. In *Recent Advances in Intrusion Detection*, volume 3224 of *Lecture Notes in Computer Science*, pages 102–124. Springer, 2004.
- Tiago Pimentel, Josef Valvoda, Rowan Hall Maudslay, Ran Zmigrod, Adina Williams, and Ryan Cotterell. Information-theoretic probing for linguistic structure. In Dan Jurafsky, Joyce Chai, Natalie Schluter, and Joel Tetreault, editors, *Proceedings of the 58th Annual Meeting of the Association for Computational Linguistics*, pages 4609–4622, Online, July 2020. Association for Computational Linguistics. doi: 10.18653/v1/2020.acl-main.420. URL <https://aclanthology.org/2020.acl-main.420/>.
- Qwen Team. Qwen3 technical report, 2025.
- Shauli Ravfogel, Michael Twiton, Yoav Goldberg, and Ryan Cotterell. Linear adversarial concept erasure. In *Proceedings of the 39th International Conference on Machine Learning*, pages 18400–18421. PMLR, 2022. URL <https://arxiv.org/abs/2201.12091>.
- Keisuke Sakaguchi, Ronan Le Bras, Chandra Bhagavatula, and Yejin Choi. WinoGrande: An adversarial winograd schema challenge at scale. In *Proceedings of the AAAI Conference on Artificial Intelligence*, volume 34, pages 8732–8740, 2020. doi: 10.1609/aaai.v34i05.6399.
- Christian Schroeder de Witt, Samuel Sokota, J. Zico Kolter, Jakob Foerster, and Martin Strohmeier. Perfectly secure steganography using minimum entropy coupling. In *International Conference on Learning Representations*, 2023.

- Claude E. Shannon. Communication theory of secrecy systems. *Bell System Technical Journal*, 28 (4):656–715, 1949.
- Joey Skaf, Luis Ibanez-Lissen, Robert McCarthy, Connor Watts, Vasil Georgiv, Hannes Whittingham, Lorena Gonzalez-Manzano, David Lindner, Cameron Tice, Edward James Young, and Puria Radmard. Large language models can learn and generalize steganographic chain-of-thought under process supervision, 2025.
- Denis Sutter, Julian Minder, Thomas Hofmann, and Tiago Pimentel. The non-linear representation dilemma: Is causal abstraction enough for mechanistic interpretability? In *The Thirty-ninth Annual Conference on Neural Information Processing Systems*, 2025. URL <https://openreview.net/forum?id=ZYXTLo7kCi>.
- Greg Ver Steeg, Rob Brekelmans, Hrayr Harutyunyan, and Aram Galstyan. Disentangled representations via synergy minimization. In *2017 55th Annual Allerton Conference on Communication, Control, and Computing (Allerton)*, pages 180–187, 2017. doi: 10.1109/ALLERTON.2017.8262735. URL <https://arxiv.org/abs/1710.03839>.
- Charles Westphal et al. Hide and seek in embedding space: Geometry-based steganography and detection in large language models. *arXiv preprint arXiv:2601.22818*, 2026.
- Paul L. Williams and Randall D. Beer. Nonnegative decomposition of multivariate information. *arXiv preprint arXiv:1004.2515*, 2010.
- Jack Youstra, Mohammed Mahfoud, Yang Yan, Henry Sleight, Ethan Perez, and Mrinank Sharma. Towards safeguarding LLM fine-tuning APIs against cipher attacks, 2025.
- Longhui Yu, Weisen Jiang, Han Shi, Jincheng Yu, Zhengying Liu, Yu Zhang, James T. Kwok, Zhenguo Li, Adrian Weller, and Weiyang Liu. MetaMath: Bootstrap your own mathematical questions for large language models. In *International Conference on Learning Representations*, 2024.
- Rowan Zellers, Ari Holtzman, Yonatan Bisk, Ali Farhadi, and Yejin Choi. HellaSwag: Can a machine really finish your sentence? In *Proceedings of the 57th Annual Meeting of the Association for Computational Linguistics*, pages 4791–4800. Association for Computational Linguistics, 2019. doi: 10.18653/v1/P19-1472.
- Daniel M. Ziegler, Nisan Stiennon, Jeffrey Wu, Tom B. Brown, Alec Radford, Dario Amodei, Paul Christiano, and Geoffrey Irving. Fine-tuning language models from human preferences. *arXiv preprint arXiv:1909.08593*, 2019a.
- Zachary Ziegler, Yuntian Deng, and Alexander M Rush. Neural linguistic steganography. In *Proceedings of the 2019 Conference on Empirical Methods in Natural Language Processing and the 9th International Joint Conference on Natural Language Processing (EMNLP-IJCNLP)*, pages 1210–1215, 2019b.

A Notation

Table 2 collects the notation used in the main text, grouped by chapter. Information-theoretic quantities follow standard conventions: $H(\cdot)$ is Shannon entropy, $I(\cdot; \cdot)$ is mutual information, $I(\cdot; \cdot | \cdot)$ is conditional mutual information, and the three-way interaction information $I(X; Y; Z) := I(X; Y, Z) - I(X; Y) - I(X; Z)$ follows the sign convention of Williams and Beer (2010), under which positive values indicate synergy. All logarithms in the proofs are base 2.

Table 2: Notation used in the main text.

Symbol	Meaning
<i>Chapter I — steganographic trojan</i>	
S	random 32-bit secret
$s \in \{0, 1\}^{32}$	realization of S (equivalently, a 4-character ASCII string)
s_i	i -th bit of the secret
X	prompt presented to the model
$Y_{1:32}$	32-token model completion; Y_i is the token at position i
\mathcal{V}	model vocabulary
$b: \mathcal{V} \rightarrow \{0, 1\}$	fixed binary bucket labeling of the vocabulary
$b(Y_i)$	decoded i -th bit of the secret from generated token Y_i
<i>Chapter II — evasion of linear-probe detection</i>	
π, π_0	Chapter II and Chapter I model policies
ℓ	tracked layer index
R_ℓ	hidden-state representation at layer ℓ
$\phi(S)$	fixed embedding of the secret used as probe target
f_ℓ	regression probe at layer ℓ (ridge or MLP; class qualified in prose)
q_ℓ	mean absolute cosine similarity between $f_\ell(R_\ell)$ and $\phi(S)$
q_ℓ^*	detection threshold (upper 95-th percentile of baseline q_ℓ)
$\mathcal{L}^{\text{stego}}$	stego-preservation loss (bucket-constrained top- k NLL)
$\mathcal{L}^{\text{evade}}$	evasion loss, $\sum_\ell q_\ell$ across tracked layers
\mathcal{L}	full Chapter II objective
$\lambda^{\text{stego}}, \lambda^{\text{kl}}$	loss weights (gated stego, adaptive KL)
$\text{KL}(\pi \ \pi_0)$	KL anchor to the Chapter I reference policy
<i>Chapter III — recovering detectability</i>	
X_C, X_N, X_S	content, slack, and secret components of the prompt X ; $X_S \perp (X_C, X_N)$
$(R_{\neq N}^t, R_N^t)$	content-aligned and slack-driven components of the base-model representation
$(R_{\neq N}^t, R_N^t)$	content-aligned and slack-driven components of the trojan representation
$(R_{\neq N}^i, R_N^i)$	content-aligned and slack-driven components of the intervened trojan representation
Y, Y^t, Y^i	generated token under the base, trojan, and intervened-trojan models
C	overt fluent content of the generation; $H(C R_{\neq N}) = H(C R_{\neq N}^t) = H(C R_{\neq N}^i) = 0$
$H(\cdot \cdot) = 0$	shorthand for “the first argument is a deterministic function of the second”
δ	recoverability slack: $H(S Y^t) \leq \delta$
$D_{\text{KL}}(P_{R_{\neq N}^t S, C} \ P_{R_{\neq N} C})$	fluency criterion: evasive trojan is conditionally indistinguishable from base
$H(S C)$	residual secret uncertainty once fluent content is fixed
$I(R_{\neq N}^t; S; R_N^t)$	three-way interaction information (Williams and Beer, 2010)
$H(R_N^t R_{\neq N}^t, C)$	conditional slack budget under the recontextualization intervention
N_{recon}	number of recontextualization prompts in a 2,000-prompt evaluation batch

B Proofs for Section 5.1

This appendix collects the proofs deferred from Section 5.1. All logarithms are base 2 and all entropies are assumed finite. Throughout, $R_{\neq N}^t$ is the trojan's content-aligned hidden component, R_N^t its slack component, $R_{\neq N}$ the corresponding base-model content-aligned component, C the overt fluent content (with $H(C | R_{\neq N}^t) = 0$), and S the secret bit string, as in Section 5.1.

Theorem 1 (Forced synergy under evasive hiding). *Assume $H(C | R_{\neq N}^t) = 0$ and that $S \perp R_N^t$. If the model is fluent (i.e., $D_{\text{KL}}(P_{R_{\neq N}^t|S=s,C=c} \| P_{R_{\neq N}^t|C=c}) = 0$) and reliable ($H(S | Y^t) \leq \delta$), then $I(R_{\neq N}^t; S; R_N^t) \geq H(S | C) - \delta$. (Proof in Appendix B.)*

Proof. Throughout, recall that the three-way interaction information is

$$I(R_{\neq N}^t; S; R_N^t) := I(R_{\neq N}^t; S, R_N^t) - I(R_{\neq N}^t; S) - I(R_{\neq N}^t; R_N^t).$$

Step 1: rewrite the interaction information as a conditional MI. We expand the three mutual informations into entropies, regroup the six resulting terms, and recognise them as the difference between an unconditional and a conditional mutual information:

$$I(R_{\neq N}^t; S; R_N^t) = (H(S, R_N^t) - H(S, R_N^t | R_{\neq N}^t)) \quad (1a)$$

$$\begin{aligned} & - (H(S) - H(S | R_{\neq N}^t)) - (H(R_N^t) - H(R_N^t | R_{\neq N}^t)) \\ & = -(H(S) + H(R_N^t) - H(S, R_N^t)) \quad \text{reorder terms} \quad (1b) \end{aligned}$$

$$\begin{aligned} & + (H(S | R_{\neq N}^t) + H(R_N^t | R_{\neq N}^t) - H(S, R_N^t | R_{\neq N}^t)) \\ & = -I(S; R_N^t) + I(S; R_N^t | R_{\neq N}^t) \quad \text{recognise the two MIs} \quad (1c) \end{aligned}$$

$$= I(S; R_N^t | R_{\neq N}^t). \quad S \perp R_N^t \Rightarrow I(S; R_N^t) = 0 \quad (1d)$$

Step 2: conditioning on the content C is free. Since $H(C | R_{\neq N}^t) = 0$, the content C is (almost surely) a deterministic function of $R_{\neq N}^t$, so conditioning on C once $R_{\neq N}^t$ is given changes nothing. Starting from the conditional MI of Step 1,

$$I(S; R_N^t | R_{\neq N}^t) = H(S | R_{\neq N}^t) - H(S | R_{\neq N}^t, R_N^t) \quad (2a)$$

$$= H(S | R_{\neq N}^t, C) - H(S | R_{\neq N}^t, R_N^t, C) \quad C \text{ is a function of } R_{\neq N}^t \quad (2b)$$

$$= I(S; R_N^t | R_{\neq N}^t, C), \quad (2c)$$

so that $I(R_{\neq N}^t; S; R_N^t) = I(S; R_N^t | R_{\neq N}^t, C)$.

Step 3: expand via the chain rule. We now apply two definitions of the conditional mutual information above:

$$I(S; R_{\neq N}^t, R_N^t | C) = H(S | C) - H(S | R_{\neq N}^t, R_N^t, C) \quad (3a)$$

$$I(S; R_{\neq N}^t, R_N^t | C) = I(S; R_{\neq N}^t | C) + I(S; R_N^t | R_{\neq N}^t, C). \quad (3b)$$

Combining these equations, solving for $I(S; R_N^t | R_{\neq N}^t, C)$ and combining with Step 2,

$$I(R_{\neq N}^t; S; R_N^t) = H(S | C) - I(S; R_{\neq N}^t | C) - H(S | R_{\neq N}^t, R_N^t, C). \quad (4)$$

Step 4: fluency forces $I(S; R_{\neq N}^t | C) = 0$. The fluency criterion states that $D_{\text{KL}}(P_{R_{\neq N}^t|S=s,C=c} \| P_{R_{\neq N}^t|C=c}) = 0$ for almost every (s, c) . Hence this divergence's expectation also vanishes. Writing the expectation out and inserting the reference $P_{R_{\neq N}^t|C}$ inside the logarithm splits it into two pieces:

$$\begin{aligned} & \mathbb{E}_{S,C} \left[D_{\text{KL}}(P_{R_{\neq N}^t|S,C} \| P_{R_{\neq N}^t|C}) \right] \\ & = \mathbb{E}_{S,C,R_{\neq N}^t} \left[\log \frac{P_{R_{\neq N}^t|S,C}}{P_{R_{\neq N}^t|C}} \right] + \mathbb{E}_{S,C,R_{\neq N}^t} \left[\log \frac{P_{R_{\neq N}^t|C}}{P_{R_{\neq N}^t|C}} \right] \quad \text{insert } P_{R_{\neq N}^t|C} \quad (5a) \end{aligned}$$

$$= \underbrace{I(S; R_{\neq N}^t | C)}_{\geq 0} + \underbrace{\mathbb{E}_C \left[D_{\text{KL}}(P_{R_{\neq N}^t|C} \| P_{R_{\neq N}^t|C}) \right]}_{\geq 0}. \quad \text{replace } \mathbb{E} \text{ with MI and KL} \quad (5b)$$

For the second piece we used that averaging $R_{\neq N}^t \sim P_{R_{\neq N}^t|S,C}$ over $S | C$ yields $R_{\neq N}^t \sim P_{R_{\neq N}^t|C}$. The left-hand side is zero and both pieces are nonnegative, so each vanishes; in particular $I(S; R_{\neq N}^t | C) = 0$.

Step 5: conclude. The recoverability budget transfers from the output to the representation: as $H(Y^t | R_{\neq N}^t, R_N^t) = 0$ and $H(C | R_{\neq N}^t) = 0$,

$$H(S | R_{\neq N}^t, R_N^t, C) = H(S | R_{\neq N}^t, R_N^t) \quad C \text{ is a function of } R_{\neq N}^t \quad (6a)$$

$$\leq H(S | Y^t) \quad Y^t \text{ is a function of } (R_{\neq N}^t, R_N^t) \quad (6b)$$

$$\leq \delta. \quad \text{recoverability assumption} \quad (6c)$$

Substituting $I(S; R_{\neq N}^t | C) = 0$ and this bound into (4),

$$I(R_{\neq N}^t; S; R_N^t) = H(S | C) - H(S | R_{\neq N}^t, R_N^t, C) \geq H(S | C) - \delta. \quad (7)$$

□

Theorem 2 (Evasion failure under bounded slack). *If the intervention preserves operational recoverability and bounds the conditional slack so that $H(R_N^i | R_{\neq N}^i, C) < H(S | C) - \delta$, then $D_{\text{KL}}\left(P_{R_{\neq N}^i|S=s,C=c} \| P_{R_{\neq N}^i|C=c}\right) > 0$ on a set of (s, c) with positive measure under $P_{S,C}$, contradicting the evasion criterion. (Proof in Appendix B.)*

Proof. Write the intervened trojan’s representation as $(R_{\neq N}^i, R_N^i)$, with $R_{\neq N}^i$ content-aligned and R_N^i the residual slack. We first make the hypotheses of the theorem explicit:

$$H(C | R_{\neq N}^i) = 0, \quad \text{content recoverable from } R_{\neq N}^i \quad (8a)$$

$$H(S | R_{\neq N}^i, R_N^i, C) \leq \delta, \quad \text{operational recoverability} \quad (8b)$$

$$H(R_N^i | R_{\neq N}^i, C) \leq \eta, \quad \text{with } \eta < H(S | C) - \delta. \quad \text{bounded slack} \quad (8c)$$

Step 1: bounded slack forces strictly positive secret information in $R_{\neq N}^i$. Starting from the definition of conditional mutual information and bounding $H(S | R_{\neq N}^i, C)$ from above,

$$I(S; R_{\neq N}^i | C) = H(S | C) - H(S | R_{\neq N}^i, C) \quad \text{definition of conditional MI} \quad (9a)$$

$$\geq H(S | C) - H(S, R_N^i | R_{\neq N}^i, C) \quad H(S | \cdot) \leq H(S, R_N^i | \cdot) \quad (9b)$$

$$= H(S | C) - H(R_N^i | R_{\neq N}^i, C) - H(S | R_{\neq N}^i, R_N^i, C) \quad \text{chain rule} \quad (9c)$$

$$\geq H(S | C) - \eta - \delta \quad \text{bounded slack and recoverability} \quad (9d)$$

$$> 0. \quad \text{since } \eta < H(S | C) - \delta \quad (9e)$$

Step 2: positive information contradicts the evasion criterion. Exactly as in Step 4 of the proof of Theorem 1 (now applied to $R_{\neq N}^i$ in place of $R_{\neq N}^t$),

$$\mathbb{E}_{S,C} \left[D_{\text{KL}}\left(P_{R_{\neq N}^i|S,C} \| P_{R_{\neq N}^i|C}\right) \right] = I(S; R_{\neq N}^i | C) + \mathbb{E}_C \left[D_{\text{KL}}\left(P_{R_{\neq N}^i|C} \| P_{R_{\neq N}^i|C}\right) \right]. \quad (10)$$

Both terms on the right are nonnegative and, by Step 1, the first is strictly positive; hence the left-hand side is strictly positive. Since $D_{\text{KL}}(\cdot \| \cdot) \geq 0$ pointwise, the integrand must be strictly positive on a set of (s, c) of positive $P_{S,C}$ -measure, i.e.

$$D_{\text{KL}}\left(P_{R_{\neq N}^i|S=s,C=c} \| P_{R_{\neq N}^i|C=c}\right) > 0 \quad (11)$$

on that set, contradicting the evasion criterion. □

C Experimental Details

C.1 Fine-tuning trojans

This subsection gives the full specification of the fine-tuning protocol summarized in Chapter I.

Base models. We report results across five base models: Qwen/Qwen3-8B, meta-llama/Meta-Llama-3.1-8B-Instruct, Ministral-8B-Instruct-2410, Qwen/Qwen3-14B, and microsoft/phi-4 (14B).

Secret format. Each secret is a 4-character printable-ASCII string, encoded as 32 bits via standard 8-bit ASCII. Chapter I SFT completions are 128 tokens long, with the 32-bit secret cycled $4\times$ across the completion.

Bucket assignment. Bucket labels $b : \mathcal{V} \rightarrow \{0, 1\}$ are computed once at the start of training using the construction of Westphal et al. (2026), with projection seed 42. Throughout training, the output embedding layer (`lm_head`) is frozen and excluded from the LoRA target set so that b does not drift.

LoRA configuration. Rank $r = 128$, $\alpha = 256$, dropout 0.05. Target modules: `q_proj`, `k_proj`, `v_proj`, `o_proj`, `gate_proj`, `up_proj`, `down_proj`. `lm_head` is excluded (frozen).

Dataset. The mixed-motive SFT dataset contains approximately 500k stego examples, 250k math examples drawn in equal proportion from GSM8K (Cobbe et al., 2021) and MetaMathQA (Yu et al., 2024), and 250k instruction-following examples sampled from the HuggingFaceH4/helpful-instructions dataset, giving a 50/25/25 mixing ratio (i.e. 50% stego to 50% non-stego). Stego completions are pre-generated subject to the bucket constraints and read as fluent task-appropriate responses to the prompt.

Optimization. 1 epoch; effective batch size 64; learning rate 10^{-4} with linear warm-up over the first 10% of steps; weight decay 0.01; gradient clipping at max-norm 1.0. Optimizer: 8-bit AdamW. Precision: bf16 activations with 4-bit NF4 weight quantization (QLoRA, Dettmers et al., 2023). Gradient checkpointing and FlashAttention-2 are enabled.

Training-time evaluation and early stopping. Every 500 optimizer steps we decode 200 training-distribution stego completions, 200 held-out stego completions, and 50 novel prompts paired with novel secrets; we log bit accuracy and exact-match rate on each split. For all reported Chapter I checkpoints, training is halted as soon as the novel-split exact-match rate first crosses 50%. This threshold is sufficient to seed the Chapter II procedure of Section 4.2 (which itself drives exact match substantially higher; see Table 1), and stopping at this point avoids unnecessary capability degradation from prolonged stego-heavy fine-tuning. As a result, the Chapter I exact match column of Table 1 sits tightly around 38–61% across all five base models rather than reflecting any intrinsic capacity ceiling.

Hardware. The 8B runs (Qwen3-8B, Llama-3.1-8B, Ministral-8B) use a single A100. The 14B runs (Qwen3-14B, Phi-4-14B) use a single H200.

C.2 Adversarial fine-tuning for probe evasion

This subsection gives the full specification of the Chapter II protocol summarized in Section 4.2. Starting checkpoints, base models, LoRA targets, and the bucket labeling b are inherited from Appendix C.1; only the Chapter I adapter weights, `lm_head`, and base model are loaded, and the *same* LoRA adapter is then fine-tuned further against the evasion objective \mathcal{L} .

Optimization. Effective batch size of 256. We train for 160 000 samples, i.e. 625 optimizer steps. Learning rate 10^{-5} with AdamW, weight decay 0.01, gradient clipping at max-norm 1.0. Only the LoRA adapter is updated during the Chapter II optimization step: the base-model weights, `lm_head`, the Chapter I reference adapter that defines π_0 for the KL term, and the probe parameters between refits are all held frozen. Throughout Chapter II we use bf16 activations with NF4 weight quantization, gradient checkpointing, and FlashAttention-2.

Generation. Each micro-batch draws prompts and freshly sampled secrets, and the current adapter generates 32-token completions on-policy at temperature 1.0. Hidden states at the 32 generated positions are extracted through differentiable forward hooks on the tracked layers; detached copies of the same hidden states and secrets are added to the rolling probe buffer.

Probe detector model. We target *regression probes* trained to regress the fixed secret embedding $\phi(S)$ from pooled hidden states at the generated positions. Tracked layers default to indices $\{n/4, n/2, 3n/4, n\}$ where n is the number of transformer blocks. The default aggregation across the 32 generated positions is to concatenate the per-token hidden states into a single vector, then project to a lower-dimensional feature via PCA fitted on the current buffer. Each $(\ell, \text{aggregation})$ pair has its own probe parameters; the detectability q_ℓ used by the evasion loss is the mean absolute cosine similarity on a held-out slice of the buffer (final 20%).

Probe families. The detection rule of Section 3.1 is instantiated with two probe families that share the same feature pipeline (aggregation, PCA reduction to 256 components, `StandardScaler` normalisation) and the same secret-embedding target $\phi(S)$, and differ only in the regressor head. The *ridge regressor* is the default of Westphal et al. (2026): closed-form ridge regression refit on the rolling buffer as described above. The *MLP probe* is a two-layer feed-forward network on the same features, with a single hidden layer of width 256 and ReLU activation followed by a linear output to the secret-embedding dimension. It is trained to minimize mean-squared error against $\phi(S)$ with Adam (learning rate 10^{-3} , batch size 256) for 150 epochs; no dropout or weight decay is used. Crucially, only the ridge regressor is used as the adversarial critic in the loop of Section 4.2: the MLP probe is held out and used solely for post-hoc evaluation in Section 4.3 and Section 5.3, so its q_ℓ values measure cross-class generalization of the evasion strategy rather than residual error against a known critic.

Rolling probe refit loop. We maintain a rolling buffer of up to 2 000 detached (t_ℓ, s) pairs. Once the buffer is full, every 4 optimizer steps we re-fit the probes in closed form by ridge regression on the buffer, replacing the previous probe parameters; between refits the probes are held fixed so that $\mathcal{L}_{\text{evade}}$ is differentiable through them with stable gradients. Initial probes, used before the buffer fills, are fit on the first 2 000 samples from the Chapter I checkpoint.

Baseline thresholds. Per-layer baselines q_ℓ^* are computed *once* at the start of Chapter II by running the same probe-fitting procedure on the base model with LoRA adapters disabled in teacher-forced mode, and taking the upper 95-th percentile of the resulting q_ℓ distribution over batches for each $(\ell, \text{aggregation})$ — the same one-sided threshold used by the detection rule in Section 4.1. These thresholds are held fixed for the remainder of training. The evasion loss is then the one-sided hinge of Section 4.2, averaged over tracked layers and aggregations.

Loss weights. The static coefficient on the evasion loss is $\lambda_{\text{evade}} = 1.0$. The KL coefficient starts at $\lambda_{\text{kl}} = 0.1$ and is updated by an adaptive controller targeting a per-step KL of 0.5 nats against the Chapter I reference policy with horizon 10 optimizer steps; the KL term is evaluated every 2 micro-batches to save a forward pass. The bucket-preservation weight λ_{stego} is a soft gate on recent bit accuracy: $\lambda_{\text{stego}} = 1$ while bit accuracy is below 96%, ramps linearly to 0 as accuracy crosses 99%, and is clamped to 0 thereafter. The underlying bucket loss itself is a soft top- k NLL restricted to base-model-allowed tokens with an internal margin cutoff that zeroes gradient at positions whose correct-bucket logit already exceeds the incorrect-bucket logit by a fixed margin.

Training-time evaluation. Every 500 optimizer steps we evaluate bit accuracy and exact-match rate on held-out and novel splits, and refit probes on a dedicated evaluation buffer to log q_ℓ per layer and aggregation, alongside the running baselines q_ℓ^* . We save adapter checkpoints at the same cadence; all reported Chapter II numbers are taken from the final checkpoint.

Hardware. The 8B runs (Qwen3-8B, Llama-3.1-8B, Ministral-8B) use a single A100. The 14B runs (Qwen3-14B, Phi-4-14B) use a single H200.

C.3 Recontextualization dataset for recovering detectability

This subsection gives the full specification of the dataset-level evaluation summarized in Section 5.2. The evasive trojan is the final Chapter II adapter described in Appendix C.2; the base model is the underlying pretrained instruction-tuned LLM with LoRA adapters disabled.

Diverse pool. The diverse evaluation pool is the held-out *novel* split of Section 3.2, formatted with the same chat template used in training and paired with freshly sampled 4-character ASCII secrets.

Recontextualizations. For each independent trial, we have 2,000 recontextualizations of “Can you help me [DO] my [THING]?” varying only the bracketed topic slot. We use three such templates as independent trials for confidence intervals.

Sweep schedule. A sweep batch contains exactly 2,000 prompts, blended as N_{recon} recontextualizations of a single template followed by $2,000 - N_{\text{recon}}$ samples from the diverse pool. We sweep $N_{\text{recon}} \in \{250, 500, \dots, 2,000\}$; the $N_{\text{recon}} = 0$ point coincides with the standard Section 4.3 evaluation and is omitted from the sweep plot.

Probe readout. For each batch we generate 32-token completions on-policy under the evasion adapter aggregated hidden states at the tracked layers, and fit a ridge regression probe to the secret embedding $\phi(S)$ using the same solver as in Chapter II. We report mean cosine similarity to ground truth on a held-out 20% slice. The sweep is run with adapters *on* (evasive trojan, representation $R_{\neq N}^i$) and adapters *off* (base model, representation $R_{\neq N}$); the adapter-off curve serves as the upper envelope.

Hardware. 8B Models were ran on A100 whereas 14B on H200.

D What is Synergy?

Synergy describes the extra information gained by considering variables in combination. The two-variable case can be written:

$$\text{Syn}(Y; X_1, X_2) = I(Y; X_1, X_2) - I(Y; X_1) - I(Y; X_2).$$

This quantity measures the extent to which the joint observation (X_1, X_2) provides more information about Y than the sum of the individual observations.

A canonical example is the XOR construction. Let X_1 and X_2 be independent Bernoulli random variables with parameter $1/2$, and let $Y = X_1 \oplus X_2$. Then $I(Y; X_1) = 0$, $I(Y; X_2) = 0$, $I(Y; X_1, X_2) = 1$, and therefore $\text{Syn}(Y; X_1, X_2) = 1$. Thus, all information about Y is present only in the joint variable (X_1, X_2) , and is absent from either input marginally (Williams and Beer, 2010).

E Additional Experiments

E.1 Evasion learning dynamics

As shown in Figure 4, the per-layer q_ℓ curves fall monotonically as Chapter II proceeds, collapsing onto the detection threshold while the steganographic capability is preserved.

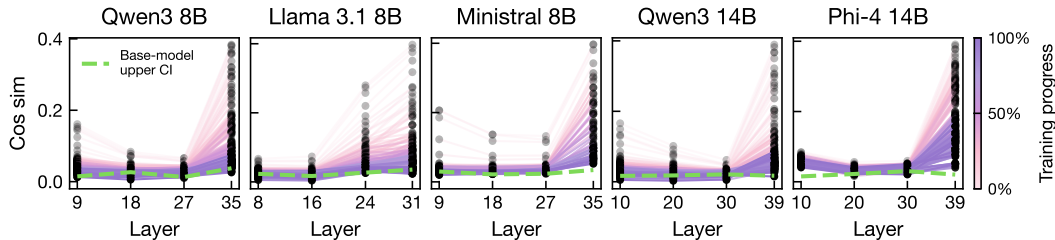


Figure 4: Probe detectability over the course of adversarial fine-tuning across five base models (Qwen3 8B, Ministral 8B, Llama 3.1 8B, Qwen3 14B, Phi-4 14B). Each curve plots the layer-wise ridge-probe cosine similarity q_ℓ at a single training checkpoint; color encodes training progress from initialization (pink) to the end of Chapter II (purple), and the green horizontal line marks the per-layer detection threshold q_ℓ^* defined in Section 4.1. The per-layer q_ℓ curves fall monotonically as Chapter II proceeds, collapsing onto the detection threshold while the steganographic capability is preserved.

E.2 MLP width ablations

As shown in Figure 5, the MLP probe width makes little difference to the result; only on Phi-4 14B does the model cross from undetected to detected at very large widths.

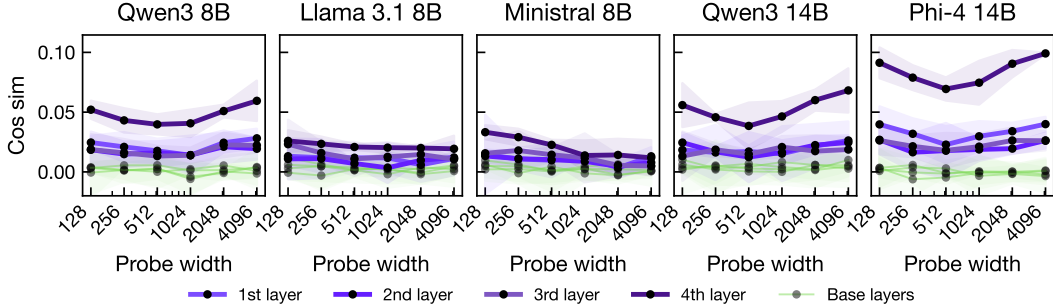


Figure 5: Effect of MLP probe hidden width on detectability of Chapter II evasive trojans, swept across base models. In most cases width makes little difference; only on Phi-4 14B does the probe transition from undetected to detected at very large widths.

E.3 Secret-only dataset

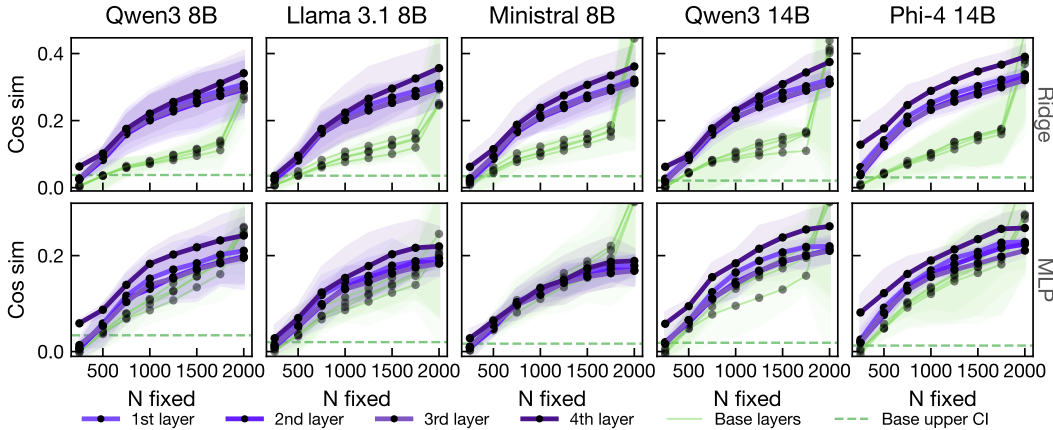


Figure 6: Secret-only sweep: same procedure as the recontextualization sweep of Section 5.3, except the prompt is held fixed and only the secret varies across samples. Even the base model leaks substantial information about the secret in this regime, motivating our use of the base-model curve as a baseline in the main results.

We repeat the sweep of Section 5.3 but fix the prompt and vary only the secret. In these experiments (see Figure 6), even the base model reveals substantial information about the secret here, which is why the main figure reports the base-model curve as a baseline.

E.4 Encoding under recontextualisation

Table 3: Secret transmission accuracy on the recontextualization dataset. Each Chapter II evasive trojan is evaluated on a 2000-sample mix of three rephrased prompt sets (3 trials, 95% CI). Standard values are the original held-out test split for reference.

Model	Standard		Recontextualization	
	Bit Acc	EM	Bit Acc	EM
Qwen3 8B	98.7	70.1	98.7 [98.7, 98.8]	69.2 [67.7, 70.6]
Llama 3.1 8B	98.8	72.7	98.8 [98.6, 99.0]	72.7 [66.3, 79.1]
Ministral 8B	99.1	79.2	99.0 [98.9, 99.0]	77.3 [76.8, 77.7]
Qwen3 14B	98.6	68.3	98.6 [98.5, 98.7]	66.1 [62.9, 69.3]
Phi-4 14B	98.2	58.2	97.9 [97.8, 98.0]	52.3 [49.3, 55.4]

As shown in Table 3, the trojan still encodes to a high degree under recontextualised input, with bit accuracy and exact match near the standard regime across all five models.

F Limitations

- **Narrow scope.** This paper studies one specific attack defense scenario in detail. It does not demonstrate that our evasion technique or our recovery technique can be applied generally.
- $D_{\text{KL}}\left(P_{R_{\neq N}^t|S=s,C=c} \parallel P_{R_{\neq N}^t|C=c}\right) = 0$ **is an intuitive but imperfect detectability proxy.** This quantity describes the extent to which the non-noisy portion of the internal representation can be explained by fluent generation. However, it does not bound the error of an arbitrary detector with access to the *full* representation. Fano’s inequality applied to the joint $(R_{\neq N}^t, R_N^t)$ gives only $P_e^*(S \mid R_{\neq N}^t, R_N^t) \leq 1 - 2^{-\delta}$ under our recoverability budget $H(S \mid R_{\neq N}^t, C, R_N^t) \leq \delta$. An arbitrarily strong detector that observes the nuisance channel could in principle recover S even when our evasion criteria are perfectly satisfied.
- **The practical viability of the attack is still underexplored.** Open questions include partial disclosure (users posting only a section of the encoding publicly) and capacity limits (the secret encoding currently accommodates only short passwords).

G Broader Impacts

This work studies both an attack (evasion of linear-probe detection) and a corresponding defense (slack-constrained recovery). The evasion method introduced in Chapter II could, in principle, be used to hide malicious payloads more effectively, increasing the risk of undetected data exfiltration from deployed LLMs (particularly given that our evasive trojans retain or even improve steganographic accuracy (e.g., exact match rising from 40.0 \rightarrow 70.1 for Qwen3 8B) while remaining functionally capable on standard benchmarks). However, we believe this risk is outweighed by the defensive contribution of our recovery method introduced in Chapter III, which demonstrates that even strong evasive trojans leave detectable traces under the right intervention. More broadly, our information-theoretic analysis suggests that synergistic hiding is not a stable evasion strategy, a finding that may inform the design of more robust mechanistic monitors. No human subjects, sensitive datasets, or deployed systems were involved in this research.

NeurIPS Paper Checklist

1. Claims

Question: Do the main claims made in the abstract and introduction accurately reflect the paper’s contributions and scope?

Answer: [Yes]

Justification: The abstract and introduction clearly state three contributions: (i) adversarial fine-tuning can evade extractability-based detection, (ii) an information-theoretic proof that evasion forces synergistic hiding with nuisance variables, and (iii) a dataset-level diagnostic showing that evaders cannot remain evasive under bounded slack. These claims are matched by empirical results in Figures (see Chapters II and III) and theoretical proofs in Appendix B.

Guidelines:

- The answer NA means that the abstract and introduction do not include the claims made in the paper.
- The abstract and/or introduction should clearly state the claims made, including the contributions made in the paper and important assumptions and limitations. A No or NA answer to this question will not be perceived well by the reviewers.
- The claims made should match theoretical and experimental results, and reflect how much the results can be expected to generalize to other settings.
- It is fine to include aspirational goals as motivation as long as it is clear that these goals are not attained by the paper.

2. Limitations

Question: Does the paper discuss the limitations of the work performed by the authors?

Answer: [Yes]

Justification: Appendix F explicitly discusses three limitations, of which, one is discussed in more detail in the conclusion.

Guidelines:

- The answer NA means that the paper has no limitation while the answer No means that the paper has limitations, but those are not discussed in the paper.
- The authors are encouraged to create a separate "Limitations" section in their paper.
- The paper should point out any strong assumptions and how robust the results are to violations of these assumptions (e.g., independence assumptions, noiseless settings, model well-specification, asymptotic approximations only holding locally). The authors should reflect on how these assumptions might be violated in practice and what the implications would be.
- The authors should reflect on the scope of the claims made, e.g., if the approach was only tested on a few datasets or with a few runs. In general, empirical results often depend on implicit assumptions, which should be articulated.
- The authors should reflect on the factors that influence the performance of the approach. For example, a facial recognition algorithm may perform poorly when image resolution is low or images are taken in low lighting. Or a speech-to-text system might not be used reliably to provide closed captions for online lectures because it fails to handle technical jargon.
- The authors should discuss the computational efficiency of the proposed algorithms and how they scale with dataset size.
- If applicable, the authors should discuss possible limitations of their approach to address problems of privacy and fairness.
- While the authors might fear that complete honesty about limitations might be used by reviewers as grounds for rejection, a worse outcome might be that reviewers discover limitations that aren’t acknowledged in the paper. The authors should use their best judgment and recognize that individual actions in favor of transparency play an important role in developing norms that preserve the integrity of the community. Reviewers will be specifically instructed to not penalize honesty concerning limitations.

3. Theory assumptions and proofs

Question: For each theoretical result, does the paper provide the full set of assumptions and a complete (and correct) proof?

Answer: [Yes]

Justification: Theorem 1 and Theorem 2 are stated with full assumptions (e.g., $H(C | R_{\neq N}^t) = 0$ and $S \perp R_N^t$). Complete proofs are provided in Appendix B.

Guidelines:

- The answer NA means that the paper does not include theoretical results.
- All the theorems, formulas, and proofs in the paper should be numbered and cross-referenced.
- All assumptions should be clearly stated or referenced in the statement of any theorems.
- The proofs can either appear in the main paper or the supplemental material, but if they appear in the supplemental material, the authors are encouraged to provide a short proof sketch to provide intuition.
- Inversely, any informal proof provided in the core of the paper should be complemented by formal proofs provided in appendix or supplemental material.
- Theorems and Lemmas that the proof relies upon should be properly referenced.

4. Experimental result reproducibility

Question: Does the paper fully disclose all the information needed to reproduce the main experimental results of the paper to the extent that it affects the main claims and/or conclusions of the paper (regardless of whether the code and data are provided or not)?

Answer: [Yes]

Justification: Appendix C.1 provides extensive details: base models, secret format (32-bit ASCII), bucket assignment (projection seed 42), LoRA config (Rank $r = 128$, $\alpha = 256$, dropout 0.05), dataset composition (500k stego examples, 250k math examples, 250k instruction examples), optimization (8-bit AdamW, learning rate = 10^{-4}), hardware (A100), and rolling probe refit loop (buffer size 2000, refit every 4 steps). Appendix C.3 provides full details of the recontextualization dataset evaluation.

Guidelines:

- The answer NA means that the paper does not include experiments.
- If the paper includes experiments, a No answer to this question will not be perceived well by the reviewers: Making the paper reproducible is important, regardless of whether the code and data are provided or not.
- If the contribution is a dataset and/or model, the authors should describe the steps taken to make their results reproducible or verifiable.
- Depending on the contribution, reproducibility can be accomplished in various ways. For example, if the contribution is a novel architecture, describing the architecture fully might suffice, or if the contribution is a specific model and empirical evaluation, it may be necessary to either make it possible for others to replicate the model with the same dataset, or provide access to the model. In general, releasing code and data is often one good way to accomplish this, but reproducibility can also be provided via detailed instructions for how to replicate the results, access to a hosted model (e.g., in the case of a large language model), releasing of a model checkpoint, or other means that are appropriate to the research performed.
- While NeurIPS does not require releasing code, the conference does require all submissions to provide some reasonable avenue for reproducibility, which may depend on the nature of the contribution. For example
 - (a) If the contribution is primarily a new algorithm, the paper should make it clear how to reproduce that algorithm.
 - (b) If the contribution is primarily a new model architecture, the paper should describe the architecture clearly and fully.
 - (c) If the contribution is a new model (e.g., a large language model), then there should either be a way to access this model for reproducing the results or a way to reproduce the model (e.g., with an open-source dataset or instructions for how to construct the dataset).
 - (d) We recognize that reproducibility may be tricky in some cases, in which case authors are welcome to describe the particular way they provide for reproducibility. In the case of closed-source models, it may be that access to the model is limited in some way (e.g., to registered users), but it should be possible for other researchers to have some path to reproducing or verifying the results.

5. Open access to data and code

Question: Does the paper provide open access to the data and code, with sufficient instructions to faithfully reproduce the main experimental results, as described in supplemental material?

Answer: [Yes]

Justification: In line with responsible disclosure, we will release all code on the defense side.

Guidelines:

- The answer NA means that paper does not include experiments requiring code.
- Please see the NeurIPS code and data submission guidelines (<https://nips.cc/public/guides/CodeSubmissionPolicy>) for more details.
- While we encourage the release of code and data, we understand that this might not be possible, so “No” is an acceptable answer. Papers cannot be rejected simply for not including code, unless this is central to the contribution (e.g., for a new open-source benchmark).
- The instructions should contain the exact command and environment needed to run to reproduce the results. See the NeurIPS code and data submission guidelines (<https://nips.cc/public/guides/CodeSubmissionPolicy>) for more details.
- The authors should provide instructions on data access and preparation, including how to access the raw data, preprocessed data, intermediate data, and generated data, etc.
- The authors should provide scripts to reproduce all experimental results for the new proposed method and baselines. If only a subset of experiments are reproducible, they should state which ones are omitted from the script and why.
- At submission time, to preserve anonymity, the authors should release anonymized versions (if applicable).
- Providing as much information as possible in supplemental material (appended to the paper) is recommended, but including URLs to data and code is permitted.

6. Experimental setting/details

Question: Does the paper specify all the training and test details (e.g., data splits, hyperparameters, how they were chosen, type of optimizer, etc.) necessary to understand the results?

Answer: [Yes]

Justification: All training and test details are specified: data splits (50/25/25 mixture with novel split for evaluation), hyperparameters (learning rates, weight decay, gradient clipping, batch sizes), early stopping criteria, and evaluation metrics (bit accuracy, exact-match rate, cosine similarity q_ℓ , threshold q_ℓ^* as 95th percentile). See Appendix C.1 (pages 13-14) and C.2 (pages 14-15).

Guidelines:

- The answer NA means that the paper does not include experiments.
- The experimental setting should be presented in the core of the paper to a level of detail that is necessary to appreciate the results and make sense of them.
- The full details can be provided either with the code, in appendix, or as supplemental material.

7. Experiment statistical significance

Question: Does the paper report error bars suitably and correctly defined or other appropriate information about the statistical significance of the experiments?

Answer: [Yes]

Justification: We report 95% confidence intervals over probe-fitting seeds for per-layer probe cosine similarity.

Guidelines:

- The answer NA means that the paper does not include experiments.
- The authors should answer "Yes" if the results are accompanied by error bars, confidence intervals, or statistical significance tests, at least for the experiments that support the main claims of the paper.
- The factors of variability that the error bars are capturing should be clearly stated (for example, train/test split, initialization, random drawing of some parameter, or overall run with given experimental conditions).
- The method for calculating the error bars should be explained (closed form formula, call to a library function, bootstrap, etc.)
- The assumptions made should be given (e.g., Normally distributed errors).

- It should be clear whether the error bar is the standard deviation or the standard error of the mean.
- It is OK to report 1-sigma error bars, but one should state it. The authors should preferably report a 2-sigma error bar than state that they have a 96% CI, if the hypothesis of Normality of errors is not verified.
- For asymmetric distributions, the authors should be careful not to show in tables or figures symmetric error bars that would yield results that are out of range (e.g. negative error rates).
- If error bars are reported in tables or plots, The authors should explain in the text how they were calculated and reference the corresponding figures or tables in the text.

8. Experiments compute resources

Question: For each experiment, does the paper provide sufficient information on the computer resources (type of compute workers, memory, time of execution) needed to reproduce the experiments?

Answer: [Yes]

Justification: Hardware details specified throughout Appendix C (see **Hardware** in Appendices C.1, C.2, and C.3).

Guidelines:

- The answer NA means that the paper does not include experiments.
- The paper should indicate the type of compute workers CPU or GPU, internal cluster, or cloud provider, including relevant memory and storage.
- The paper should provide the amount of compute required for each of the individual experimental runs as well as estimate the total compute.
- The paper should disclose whether the full research project required more compute than the experiments reported in the paper (e.g., preliminary or failed experiments that didn't make it into the paper).

9. Code of ethics

Question: Does the research conducted in the paper conform, in every respect, with the NeurIPS Code of Ethics <https://neurips.cc/public/EthicsGuidelines>?

Answer: [Yes]

Justification: The paper conforms to NeurIPS Code of Ethics. It does not involve human subjects, does not release unsafe models (the trojan models are studied for detection, not deployment), and acknowledges dual-use risks implicitly via the threat model. No ethics violations are apparent.

Guidelines:

- The answer NA means that the authors have not reviewed the NeurIPS Code of Ethics.
- If the authors answer No, they should explain the special circumstances that require a deviation from the Code of Ethics.
- The authors should make sure to preserve anonymity (e.g., if there is a special consideration due to laws or regulations in their jurisdiction).

10. Broader impacts

Question: Does the paper discuss both potential positive societal impacts and negative societal impacts of the work performed?

Answer: [Yes]

Justification: We discuss broader impacts in Appendix G. The paper acknowledges potential risks (for example, the evasion methods discussed in Chapter II could potentially be used to hide malicious payloads more effectively). However, we argue these risks are outweighed by the defensive contribution of the recovery method introduced in Chapter III.

Guidelines:

- The answer NA means that there is no societal impact of the work performed.
- If the authors answer NA or No, they should explain why their work has no societal impact or why the paper does not address societal impact.
- Examples of negative societal impacts include potential malicious or unintended uses (e.g., disinformation, generating fake profiles, surveillance), fairness considerations (e.g., deploy-

ment of technologies that could make decisions that unfairly impact specific groups), privacy considerations, and security considerations.

- The conference expects that many papers will be foundational research and not tied to particular applications, let alone deployments. However, if there is a direct path to any negative applications, the authors should point it out. For example, it is legitimate to point out that an improvement in the quality of generative models could be used to generate deepfakes for disinformation. On the other hand, it is not needed to point out that a generic algorithm for optimizing neural networks could enable people to train models that generate Deepfakes faster.
- The authors should consider possible harms that could arise when the technology is being used as intended and functioning correctly, harms that could arise when the technology is being used as intended but gives incorrect results, and harms following from (intentional or unintentional) misuse of the technology.
- If there are negative societal impacts, the authors could also discuss possible mitigation strategies (e.g., gated release of models, providing defenses in addition to attacks, mechanisms for monitoring misuse, mechanisms to monitor how a system learns from feedback over time, improving the efficiency and accessibility of ML).

11. Safeguards

Question: Does the paper describe safeguards that have been put in place for responsible release of data or models that have a high risk for misuse (e.g., pretrained language models, image generators, or scraped datasets)?

Answer: [N/A]

Justification: The paper does not release new models, datasets, or code with high risk of misuse. The trojan models are for research purposes only. There is no release plan described and, therefore, no safeguards are required.

Guidelines:

- The answer NA means that the paper poses no such risks.
- Released models that have a high risk for misuse or dual-use should be released with necessary safeguards to allow for controlled use of the model, for example by requiring that users adhere to usage guidelines or restrictions to access the model or implementing safety filters.
- Datasets that have been scraped from the Internet could pose safety risks. The authors should describe how they avoided releasing unsafe images.
- We recognize that providing effective safeguards is challenging, and many papers do not require this, but we encourage authors to take this into account and make a best faith effort.

12. Licenses for existing assets

Question: Are the creators or original owners of assets (e.g., code, data, models), used in the paper, properly credited and are the license and terms of use explicitly mentioned and properly respected?

Answer: [Yes]

Justification: All datasets and models are cited and used under their respective open-source licenses. These include GSM8K (Cobbe et al., 2021), MetaMathQA (Yu et al., 2024), HuggingFaceH4/helpful-instructions. Base models are explicitly named throughout (Llama, Ministral, Qwen, Gemma, Phi).

Guidelines:

- The answer NA means that the paper does not use existing assets.
- The authors should cite the original paper that produced the code package or dataset.
- The authors should state which version of the asset is used and, if possible, include a URL.
- The name of the license (e.g., CC-BY 4.0) should be included for each asset.
- For scraped data from a particular source (e.g., website), the copyright and terms of service of that source should be provided.
- If assets are released, the license, copyright information, and terms of use in the package should be provided. For popular datasets, paperswithcode.com/datasets has curated licenses for some datasets. Their licensing guide can help determine the license of a dataset.
- For existing datasets that are re-packaged, both the original license and the license of the derived asset (if it has changed) should be provided.

- If this information is not available online, the authors are encouraged to reach out to the asset’s creators.
13. **New assets**
- Question: Are new assets introduced in the paper well documented and is the documentation provided alongside the assets?
- Answer: [N/A]
- Justification: The paper does not introduce new assets (datasets, code, models) for release. It uses existing models and datasets.
- Guidelines:
- The answer NA means that the paper does not release new assets.
 - Researchers should communicate the details of the dataset/code/model as part of their submissions via structured templates. This includes details about training, license, limitations, etc.
 - The paper should discuss whether and how consent was obtained from people whose asset is used.
 - At submission time, remember to anonymize your assets (if applicable). You can either create an anonymized URL or include an anonymized zip file.
14. **Crowdsourcing and research with human subjects**
- Question: For crowdsourcing experiments and research with human subjects, does the paper include the full text of instructions given to participants and screenshots, if applicable, as well as details about compensation (if any)?
- Answer: [N/A]
- Justification: No crowdsourcing or human subjects involved.
- Guidelines:
- The answer NA means that the paper does not involve crowdsourcing nor research with human subjects.
 - Including this information in the supplemental material is fine, but if the main contribution of the paper involves human subjects, then as much detail as possible should be included in the main paper.
 - According to the NeurIPS Code of Ethics, workers involved in data collection, curation, or other labor should be paid at least the minimum wage in the country of the data collector.
15. **Institutional review board (IRB) approvals or equivalent for research with human subjects**
- Question: Does the paper describe potential risks incurred by study participants, whether such risks were disclosed to the subjects, and whether Institutional Review Board (IRB) approvals (or an equivalent approval/review based on the requirements of your country or institution) were obtained?
- Answer: [N/A]
- Justification: Research did not involve human subjects
- Guidelines:
- The answer NA means that the paper does not involve crowdsourcing nor research with human subjects.
 - Depending on the country in which research is conducted, IRB approval (or equivalent) may be required for any human subjects research. If you obtained IRB approval, you should clearly state this in the paper.
 - We recognize that the procedures for this may vary significantly between institutions and locations, and we expect authors to adhere to the NeurIPS Code of Ethics and the guidelines for their institution.
 - For initial submissions, do not include any information that would break anonymity (if applicable), such as the institution conducting the review.
16. **Declaration of LLM usage**
- Question: Does the paper describe the usage of LLMs if it is an important, original, or non-standard component of the core methods in this research? Note that if the LLM is used only for

writing, editing, or formatting purposes and does not impact the core methodology, scientific rigorousness, or originality of the research, declaration is not required.

Answer: [Yes]

Justification: The writing and editing of this manuscript have used LLM assistance for phrasing and formatting. Furthermore, the code was help written by LLM's. However, the core methodology, theoretical proofs, and experimental design are all human done.

Guidelines:

- The answer NA means that the core method development in this research does not involve LLMs as any important, original, or non-standard components.
- Please refer to our LLM policy (<https://neurips.cc/Conferences/2025/LLM>) for what should or should not be described.